Journal of Applied Physics

REVIEW ARTICLE | DECEMBER 02 2022

Programming material properties by tuning intermolecular bonding

Upamanyu Ray ; Zhenqian Pang ; Teng Li

Journal of Applied Physics 132, 210703 (2022)
https://doi.org/10.1063/5.0123058

Journal of Applied Physics REVIEW scitation.org/journal/jap

Programming material properties by tuning intermolecular bonding

Cite as: J. Appl. Phys. **132**, 210703 (2022); doi: 10.1063/5.0123058
Submitted: 19 September 2022 · Accepted: 10 November 2022 ·
Published Online: 2 December 2022

Upamanyu Ray, Zhenqian Pang,[a] and Teng Li[a]

AFFILIATIONS

Department of Mechanical Engineering, University of Maryland College Park, Maryland 20742, USA

[a]**Authors to whom correspondence should be addressed:** zqpang@umd.edu and lit@umd.edu

ABSTRACT

Conventional strategies for materials design have long been used by leveraging primary bonding, such as covalent, ionic, and metallic bonds, between constituent atoms. However, bond energy required to break primary bonds is high. Therefore, high temperatures and enormous energy consumption are often required in processing and manufacturing such materials. On the contrary, intermolecular bonds (hydrogen bonds, van der Waals forces, electrostatic interactions, imine bonds, etc.) formed between different molecules and functional groups are relatively weaker than primary bonds. They, thus, require less energy to break and reform. Moreover, intermolecular bonds can form at considerably longer bond lengths between two groups with no constraint on a specific bond angle between them, a feature that primary bonds lack. These features motivate unconventional strategies for the material design by tuning the intermolecular bonding between constituent atoms or groups to achieve superior physical properties. This paper reviews recent development in such strategies that utilize intermolecular bonding and analyzes how such design strategies lead to enhanced thermal stability and mechanical properties of the resulting materials. The applications of the materials designed and fabricated by tuning the intermolecular bonding are also summarized, along with major challenges that remain and future perspectives that call for further attention to maximize the potential of programming material properties by tuning intermolecular bonding.

I. INTRODUCTION

Bonding between constituent atoms/molecules is crucial in designing engineering materials with desirable properties. Conventional material design strategies by leveraging primary bonding between constituent atoms are well established to design materials such as metals, ceramics, and alloys.[1–9] Primary bonds can be broadly classified into three types: covalent bonds, ionic bonds, and metallic bonds. Covalent bonds usually occur between atoms of non-metals, such as carbon [Fig. 1(a)], where electrons are shared between neighboring atoms (e.g., the four electrons in the outermost valence shell of a carbon atom). To achieve the energetically favorable configuration (octet), a carbon atom may share those four electrons with one electron from the neighboring carbon atom and three electrons from each of the three surrounding hydrogen atoms, thus forming four different covalent bonds. Ionic bonds [Fig. 1(b)] occur when there is a large difference in electronegativity in neighboring atoms. For example, sodium (Na) possesses just one electron in its outermost shell, and to achieve the stable octet configuration, it donates this electron, thus becoming a positively charged cation (Na^+). On the other hand, chlorine (Cl) possesses seven electrons in its outermost valence shell. It achieves the energetically favorable configuration by gaining that electron, thus becoming a negatively charged anion (Cl^-). An ionic bond is formed between Na^+ and Cl^- upon the transfer of the valence electron. Metallic bonds are formed when highly electrically conductive metals release their electrons from the inner valence band to the outer conduction band, thus becoming metallic cations [Fig. 1(c)], forming negatively charged free electrons (electron cloud) around them. This attraction between the positively charged metallic cation with the swarm of negatively charged electron clouds forms the metallic bond. Tuning the primary bonds between constituent atoms/molecules has been the focus of engineering materials design to achieve desired physical properties such as high strength, stiffness, toughness, thermal stability, etc. However, such desirable performances come at a price. The upper range for bond energy in primary bonds is relatively high at around 1000 kJ/mol (~1000 kJ/mol for covalent bonds, ~800 kJ/mol for ionic bonds, and ~850 kJ/mol for metallic bonds). On one hand, the high bond energy of primary

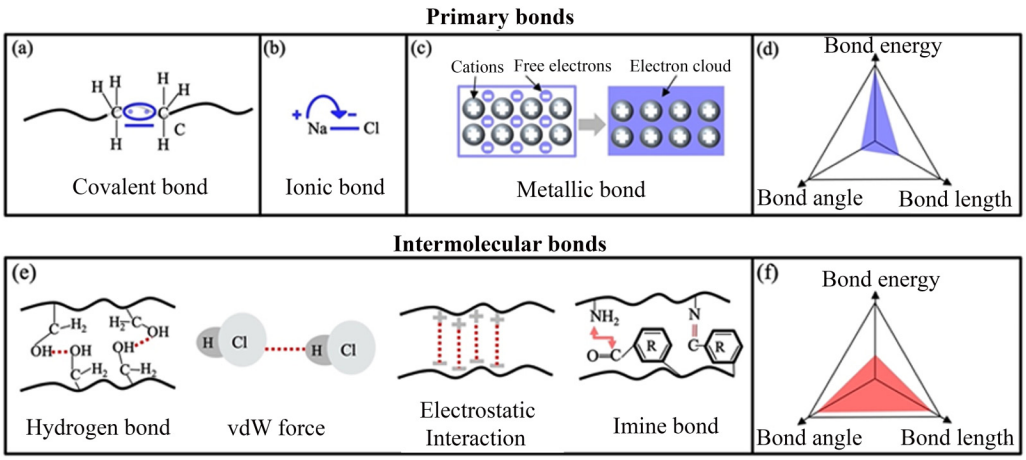

FIG. 1. Comparison between primary bonds (a)–(d) and intermolecular bonds (e) and (f). (a) Covalent bond; (b) ionic bond; (c) metallic bond; (e) Selected types of intermolecular bonds such as hydrogen bond, van der Walls (vdW) force, electrostatic interaction, and dynamic imine bond. (d) and (f) Comparison between primary bonds and intermolecular bonds in terms of bond energy, bond angle, and bond length.

bonds is the origin of many desirable physical properties of metals, ceramics, and alloys. But on the other hand, it also requires high temperature and enormous energy consumption in processing and manufacturing such materials, which often causes detrimental effects on the environment and poses challenges to sustainability and climate. For example, steel production releases more than 3×10^9 metric tons of carbon dioxide yearly, accounting for 8% of all human-made greenhouse gas emissions.

Intermolecular bonds, such as hydrogen bonds, van der Waals (vdW) forces, electrostatic interactions, imine bonds, etc., have relatively lower bond energy compared with primary bonds [Figs. 1(d) and 1(f)], the maximum value ranging around ~470 kJ/mol (~1–190 kJ/mol for hydrogen bonds, ~5–200 kJ/mol for electrostatic interactions, ~1–50 kJ/mol for van der Waals forces, and 70–470 kJ/for imine bonds).[10] So, intermolecular bonds can readily form, break, and reform under the influence of external forces when two compatible atoms or functional groups are in close proximity to each other. For example, a mechanically robust, self-healing, low-weight polymer can be designed by tuning the cross-linking density, which could rapidly heal multiple times without noticeable deformation.[11] This rapid healing is possible because the range of bond length in intermolecular bonds is much higher than the conventional primary bonds [Fig. 1(d)]. In addition to the higher bond energy described above, since the range of bond length in primary bonds is smaller, their ability to reform and reconnect decreases considerably. Furthermore, primary bonds need to be formed at a specific range of bond angles in addition to the constraint already imposed by the relatively shorter bond length. Even when the atoms are within the bond length, a primary bond cannot form if the criteria related to the specific range of bond angle are not satisfied. However, intermolecular bonds can form at a wide range of bond angles[12,13] because of their ability to reconnect at all degrees of freedom with the surrounding molecules across all three dimensions. As a result, unconventional material properties that were previously impossible using solely primary bonds can be realized by tuning intermolecular bonds. For example, the conflict between strength and toughness, which are conventionally two mutually exclusive mechanical properties, could be overcome in cellulose-based materials[14–17] that can achieve both high strength and toughness through design strategies involving spatially dense intermolecular bonds present in the constituent cellulose molecular chains.[18] A long-standing quandary, the stiffness-toughness conflict, was also recently resolved through physical cross-linking in polymer, implementing a unique application of intermolecular interactions resulting in superb material physical properties.[19] Thus, conceiving novel material design strategies to achieve unconventional yet desirable properties possess promising potential in designing next-generation high-performance materials, which asserts the need to explore the fundamental mechanism behind the strategies related to tuning of intermolecular bonds.

Intermolecular bonds can be broadly categorized into hydrogen bonding, vdW forces, electrostatic interactions, and some dynamic cross-linked bonds in between molecules, such as imine bonds, as illustrated in Fig. 1(e). The term hydrogen bond was conceptualized as early as 1912[20] but imaging evidence of intermolecular hydrogen bonding was first obtained in 2013.[21] A hydrogen bond is primarily a dipole–dipole interaction, which is formed when a hydrogen (H) is covalently bound to an atom or group having higher electronegativity. This will typically comprise elements such as oxygen (O), nitrogen (N), and fluorine (F). The atoms or groups containing these atoms are considered donors (Do), and the hydrogen covalently bonded to it is denoted by Do–H. When this group (Do–H) comes in proximity with another electronegative atom or groups having a lone pair of electrons (namely, the acceptor denoted by Ac), this forms a hydrogen bond, denoted by Do-H–Ac, where the dashed line suggests the presence of hydrogen bond. For example, a hydrogen atom (–H) in a molecular chain [Fig. 1(e), left schematic] can form hydrogen bonding with

the electronegative oxygen (–O) in a different (intermolecular hydrogen bonding) molecular chain. The energy and the geometry of the hydrogen bond can vary depending on the nature of Do and Ac. It has been proven to exist in DNA,[22,23] chitosans,[24] proteins,[25] alcohols (e.g., ethanol and methoxymethane),[26–28] natural (e.g., cellulose),[29–31] and synthetic (e.g., nylon and aramid fibers)[32,33] polymers.

Similar to hydrogen bonding, vdW forces also involve dipole–dipole interactions. However, they are weaker than hydrogen bonds and act between neutral molecules [e.g., HCl as in Fig. 1(e) titled "vdW force"]. When neutral molecules come closer within a threshold distance, electrons of one molecule are pulled toward the nucleus of another, thus delocalizing them. When the neutral molecules are within a threshold distance, repulsion occurs, thus maintaining the intermolecular distance. During the vibration or motion of the molecule, this intermolecular interaction may disassociate, causing the electrons to be delocalized. Without vdW forces, molecules would simply drift away from each other, causing a gaseous phase. A prominent example of vdW forces can be found in graphite, in which graphene layers are held together by weak vdW forces.[34–36] Typically, vdW forces vary inversely with the distance between the interacting molecules.

Electrostatic interactions, another type of non-covalent intermolecular bonding[37] occurs when opposite charges (positive or negative) are separated either due to ionization or incorporation of another ionic species [Fig. 1(e), schematic titled "Electrostatic interaction"]. These interactions might be repulsive (between like charges) and attractive (between opposite charges). For example, metal organic frameworks (MOFs) are positively charged[38] when the pH of the solution is lesser than the point of zero charge (*pzc*). Hydrated H_3O^+ ions are present; thereby, the MOFs move toward the negatively charged toxic elements (TEs), resulting in attractive electrostatic interaction. However, when the pH of the solution is greater than *pzc*, the MOFs are negatively charged, whereas the TEs are positively charged, resulting in a repulsive electrostatic interaction. Electrostatic interactions can be much stronger than vdW force and hydrogen bonding. Similar to vdW force, electrostatic interactions are long-range, and the interaction decreases gradually with respect to the distance ($1/r^2$; r is the distance between two charged elements). The electrostatic force is the primary bonding between macromolecules such as MOFs, protein, RNA, DNA, and charged particles. Additionally, the electrostatic force is predominantly influenced by the water, salt concentration, and PH.

Other dynamic cross-linked intermolecular bonds can also occur in composites, and one such example is an imine bond. Imine bonds have bond energies lower than primary covalent bonds but higher than other intermolecular bonding such as hydrogen bonds, electrostatic interactions, and π–π stacking.[10] Imine bonds [Fig. 1(e), schematic titled "Imine bonds"] are formed through a reversible process when the nucleophilic addition of primary amine (–NH_2–R) takes place with the carbonyl group (O═C–R) present in a ketone or aldehyde functional group, followed by proton transfer and acid protonation, which results in the formation of the iminium ion (–N^+ ═ C–R) with the elimination of water. The final stage is the deprotonation of nitrogen to form imine bonds (–N ═ C–R), as shown in Fig. 1(e) (schematic titled "Imine bonds"). Some other types of dynamic cross-linked bonds also exist in the form of hydrazone bonds, disulfide bonds, and oxime bonds. These dynamic cross-linked bonds are widely used in materials requiring self-healing properties.[39,40] For the scope of this review, since the discussion is based primarily on the influence of intermolecular bonds on major physical properties such as thermal stability and material mechanics, the focus of studies related to dynamic cross-linked bonds is primarily placed on imine bonds unless otherwise mentioned.

The rest of this review paper is organized as follows. Section II describes the corresponding material design strategies leveraging intermolecular bonding. Section III analyzes the influence of intermolecular bonding on thermal stability and mechanical properties. Section IV describes the applications of the materials that are fabricated by tuning the intermolecular bonding through the approaches that have been described in Sec. III. Finally, Sec. V concludes with general remarks on the areas that require immediate focus related to this domain, along with the major challenges that call for further attention.

II. MATERIAL DESIGN STRATEGIES LEVERAGING INTERMOLECULAR BONDING

Due to the weak and long-range force of these non-covalent bonding, the materials present an outstanding perspective to modify the intermolecular interactions and tailor the properties of materials. Intercalation is the insertion of an ion or a molecule into materials with layered structures, thus increasing the layer spacing and consequently enhancing the physical properties of the bulk material.[41] Typically, it is analyzed by diffraction techniques and/or by measuring electrical conductivity. A classic example of using ion intercalation techniques may be found in graphite. Pang *et al.*[35] inserted lithium (Li) ions in between the graphene layers of the bulk graphite and obtained around seven times increase in the inter-graphene-layer friction than that present in the natural graphite. Seidl *et al.*[42] analyzed in detail the reversible intercalation of solvated sodium (Na) ions into graphite which may aid in the development of future generation Na-based batteries. The strategies encompassing intercalation are not necessarily limited only to ions. They can also be extended to using polymers as the intercalating agents in metal dichalcogenides such as Molybdenum Disulfide (MoS_2), as demonstrated by Feng *et al.*[43] Here, various polymers (e.g., polyethyleneimine and polyethylene glycol) were intercalated into MoS_2 interlayers, thus expanding them. The expanded interlayer, acting as electrodes, had more active sites available for chemical reaction and allowed efficient diffusion of ions back and forth. As a result, the MoS_2/N-doped carbon heteroaerogel exhibited ultrahigh capacitance and superior cycling stability. This might be beneficial for implementation in future energy storage devices, thus elevating the importance of novel intercalation strategies.

Another method of subjecting the molecules in a material to different modes of intermolecular bonding is through element or solution replacement and incorporation of functional groups. Element or solution replacement applies to oxidative/reductive chemical reactions by which one element in a molecule is replaced by another. In addition, this may also imply treating the precursor material through a series of experiments involving chemical treatments by alcohol/enzymes followed by sonication, homogenization,

and/or centrifugation.[31,44–47] For example, the TEMPO/NaBr/NaClO oxidation of native celluloses in water[48,49] under suitable conditions will oxidize the C6-primary hydroxy groups (–CH_2OH) present on crystalline cellulose microfibril surfaces to sodium C6-carboxylate groups (–NaCOOH). As a result, there is more repulsion in the molecules which stabilizes the structure, and the resulting solution becomes well dispersed. This solution can be used as a precursor and, when hybridized with effective functional groups, may lead to the development of multiple promising high-tech materials used as filaments for osmotic energy conversion,[50] 3D printing ink,[51] high-performance separators for lithium-ion batteries,[52] biosensors for enzyme detection,[53] macrofibers for flexible supercapacitors,[54] and intelligent food packaging films.[55]

Other strategies such as cross-linking[56] may also be incorporated to enhance the interfacial adhesion between the constituent molecules without significantly altering the chemical structure. This may be implemented to design the material topology by modifying the functional groups and fabricating high-performance functional materials. In addition, separate strategies such as physical and chemical cross-linking may also be used to develop engineered materials with superior physical properties. Physical cross-linking is formed by ionic interactions or metal coordination or hydrogen bonding[57,58] and is reversible in nature, i.e., they can be dissociated or associated depending on the external stimulus (e.g., heat). The structural morphology of a material may be designed so that physical cross-linking between neighboring is effectuated. For example, when cellulose molecular chains are involved in sliding relative to each other during tensile loading, it involves breaking and reforming physically cross-linked bonds. Chemical cross-linking is frequently used where molecules (cross-linkers) consisting of multiple reactive ends attach to the functional groups of neighboring polymeric molecules, thus introducing a covalent bond between them.[59,60] They are much more stable than physical cross-linking and form a tight network by reducing the mobility of the chemically cross-linked molecular chains, which makes it difficult to sever the linked bonds. Sometimes a series of chemical and/or physical treatments may inflict a combination of a double network[61–63] of both physical and chemical cross-linking, which also leads to improved physical properties in the material.

III. INFLUENCE OF INTERMOLECULAR BONDING ON THE MATERIAL PHYSICAL PROPERTIES

This section summarizes the effects of intermolecular bonds on various physical properties of materials, such as thermal stability, mechanical strength, toughness and stiffness.

A. Thermal stability

Chemical and physical treatments for engineering the intermolecular bonding in composites can be an effective method to significantly improve their thermal stability, thus making it suitable in many large-scale industrial applications where high-temperature material endurance is of prime importance. This subsection discusses the influence of various types of intermolecular bonding, such as hydrogen bonds and imine bonds, in significantly improving the thermal stability in composites for different material types such as hydrogels, aerogels, and composite films.

For example, a strategy of tuning the intermolecular bonds to increase the thermal stability of hydrogel can be envisioned by utilizing directed hydrogen bonding, along with hydrophobicity for polymers based on β-helical polyisocyanotripeptides (TriPIC) as proposed by Yuan *et al.*[64] Synthetic polymers like TriPIC exhibit exceptionally high thermal stability owing to their structure, as shown in Fig. 2(a). The central polyisocyanide backbone [bold red in Fig. 2(a)] possesses two amide groups adjacent to it, which forms two parallel intermolecular hydrogen bonding arrays A and B [Fig. 2(a), top panel]. During heating, the hydrogen bonding network A remains stable and shields the central backbone from water, thus forming a hydrophobic core. The second intermolecular hydrogen bonding network B gets stretched on heating, thus inflicting the central polymer backbone with a helical structure with enhanced stiffness. Heating beyond lower critical solution temperature dehydrates the oligo (ethylene glycol) tails, which results in bundle formation in the polymer network, rendering high thermal stability of the hydrogels for multiple hours at 80 °C as validated by Fig. 2(b). On heating using a rheometer, the storage modulus (G'), the ratio of applied stress to measured strain increases indicating enhanced gel stiffness, which further retains its value for over 10 h at a high temperature of 80 °C. For networks with different concentrations of the TriPIC polymer, the storage modulus was observed to prominently increase from the gelation temperature [bottom point of a sudden rise in each curve in Fig. 2(c) indicating hydrogel formation] with the highest stiffness for the polymer network with maximum concentration (4 gm^{-1}) as shown in Fig. 2(b). Polymers with different concentrations were much stiffer and retained their exceptional thermal stability at 80 °C. This strain stiffening behavior is completely reversible in cooling the sample. Repeated thermal cycles have negligible effects on the other parameters, such as the mechanical properties of these hydrogels, further highlighting the effectiveness of this design principle. To shed further insights on how the bundle formation aids in thermal stability for these hydrogels, FTIR measurements were performed [Fig. 2(d)]. The intermolecular hydrogen bonds formed by amides titled "A" had the maximum intensities for –C═O– during vibrations, indicating their probable role in protecting the central polymer backbone. In contrast, the intermolecular hydrogen bonds formed by amides titled "B" maintain the backbone helix and the structural stiffness, which in turn makes the structure thermally stable. The FTIR curves for variable temperatures [different colors, Fig. 2(d)] display a change in the –C═O– vibrations, indicating its adjustment to the ambient conditions to render superior thermal stability in the bulk composite. This innovative biological approach of utilizing hydrogen bonds and hydrophobic interactions is thus effective. It may replace conventional strategies of altering the electrostatic interactions of the surface for the material to be stable against excess thermal energy. Several other research investigations also report the advantages of intermolecular bonds in enhancing the thermal stability of the hydrogel class of materials, such as in boron nitride/polyvinyl alcohol (PVA) hydrogel,[65] double-network PU-based hydrogels,[63] and in PVA-based hydrogels having nanofibrillated cellulose (NFC) aldehyde cross-linkers.[66]

Besides hydrogels, engineering the intermolecular bonding to improve thermal stability has also been demonstrated in other soft materials, such as aerogel. For example, Song *et al.*[67] fabricated a

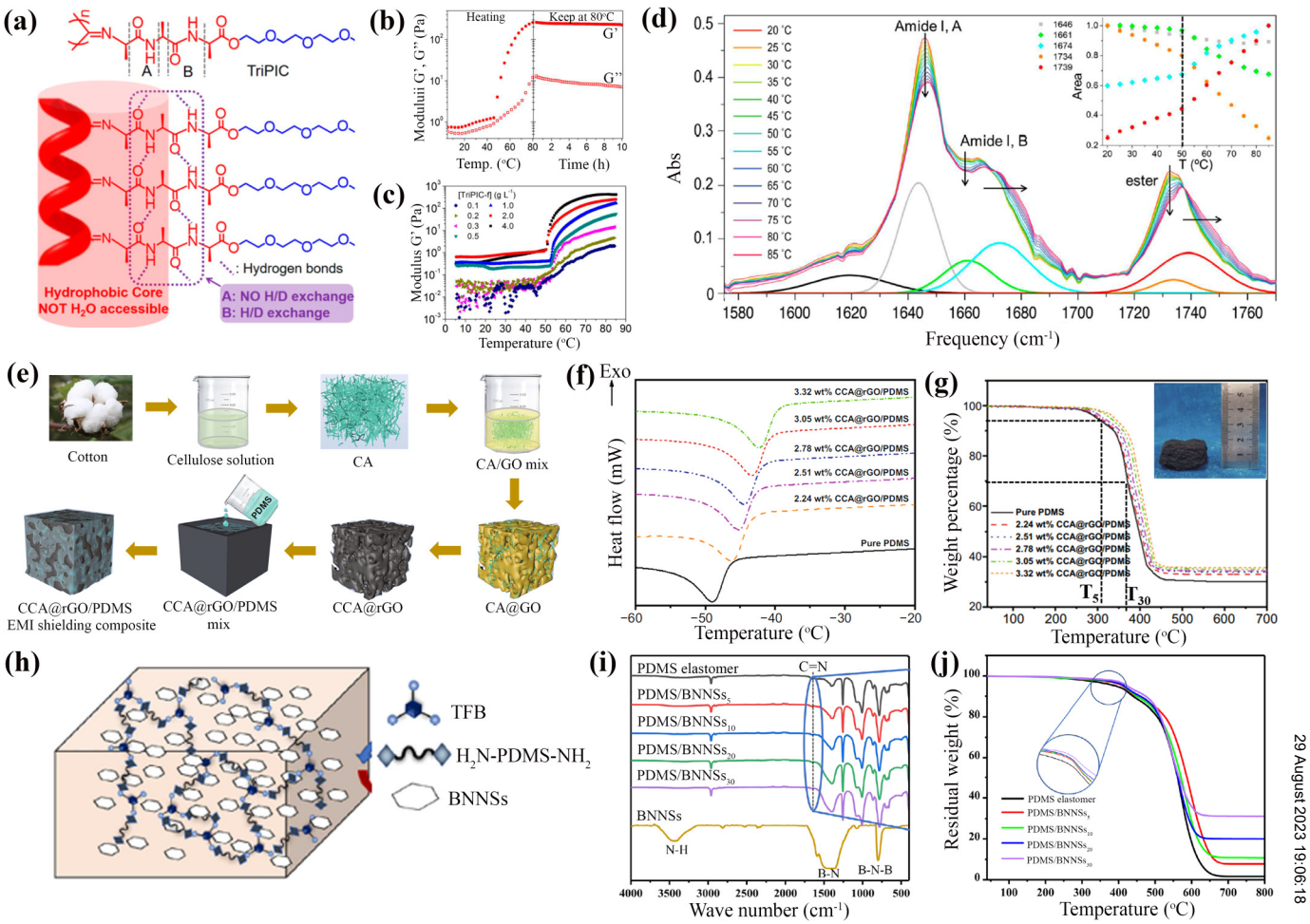

FIG. 2. Role of intermolecular bonds in improving the thermal stability of (a)–(d) hydrogels, (e)–(g) aerogels, and (h)–(j) composite films. (a) A schematic of the molecular structure of hydrogels based on β-helical polyisocyanotripeptides (TriPIC), clearly showing the central backbone (bold red) with two parallel intermolecular hydrogen bonding arrays A and B. (b) Linear rheological analysis (time sweep) when the TriPIC hydrogel is heated to 80 °C and then conditioned at 80 °C for 10 h, where G′ and G″ are the storage and loss modulus, respectively. (c) Plots of G′ with respect to temperature for different concentrations of the TriPIC hydrogel. (d) FTIR spectra of TriPIC hydrogel where the different colored lines represent each spectrum at different temperatures. (e) Schematic illustrating the fabrication process of cellulose carbon and reduced graphene-oxide polydimethylsiloxane (PDMS) aerogel (CCA@rGO/PDMS). (f) Differential scanning calorimetry (DSC) curves to obtain the glass transition temperature (T_g) for different concentrations of CCA@rGO/PDMS aerogels. (g) Thermo gravimetric analysis (TGA) plots to evaluate T_5 and T_{30} (marked by dashed lines), which, along with T_g are used to compute the heat resistance index to determine the thermal stability of the aerogel. (h) Illustration of the molecular structure of polydimethylsiloxane (PDMS)/boron nitride nano sheets (BNNS) based elastomer composite film (PDMS/BNNS). (i) FTIR spectra comparison of the PDMS/BNNS for different contents of BNNS, with pure PDMS elastomer. (j) TGA plots of the PDMS/BNNS film for different contents of BNNS and pure PDMS elastomer. (a)–(d) From Yuan *et al.*, Macromolecules **50**, 9058–9065 (2017). Copyright 2017 Author(s), licensed under a Creative Commons Attribution (CC BY) license. (e)–(g) From Song *et al.*, Nano-Micro Lett. **13**, 91 (2021). Copyright 2021 Author(s), licensed under a Creative Commons Attribution (CC BY) license. (h)–(j) Reproduced with permission from Shang *et al.*, Polym. Adv. Technol. **32**, 4745–4754 (2021). Copyright 2021 Wiley.

cellulose carbon and reduced graphene-oxide polydimethylsiloxane (PDMS) aerogel (CCA@rGO/PDMS) which showed exceptional thermal stability on increasing wt. % of cellulose in the cellulose carbon aerogel (CCA) from 2.24 wt. % to 3.95 wt. %. Here, cotton is dissolved in the cellulose solution [Fig. 2(e)] using intermolecular hydrogen bonding assisted assembly of cellulose and sodium hydroxide (NaOH)/ urea solution. Cellulose aerogels are thereby obtained through gelation and freeze-drying. The CCA@rGO are obtained through a sequence of steps involving vacuum impregnation, freeze-drying, and thermal annealing. Finally, the CCA@rGO/PDMS aerogel is prepared by pouring PDMS into the CCA@rGO mold followed by vacuum impregnation and natural cooling to room temperature. Different concentrations of CCA@rGO were impregnated in the PDMS solution to obtain CCA@rGO/PDMS

aerogels with various cellulose concentrations. More cellulose wt. % may indicate more efficient self-assembly of the solution driven by spatially denser intermolecular hydrogen bonds. To obtain the glass transition temperature (T_g) of the different concentrations of CCA@rGO/PDMS aerogels, differential scanning calorimetry (DSC) curves were plotted [Fig. 2(f)]. Here, T_g was obtained by the corresponding temperature of the trough of the curve. T_g gradually increases with an increase in the loading of CCA@rGO. For loading of CCA@rGO at 3.05 wt. %, the T_g was ~5.7 °C more than that of pure PDMS, which was fabricated without intermolecular hydrogen bonding assisted self-assembly. Since T_g indicates the phase alteration of a material from rigid solid to rubbery state, higher T_g signifies delay of the material transformation to its rubbery state, which in turn decreases the weight loss % when that material is heated to higher temperatures, as shown in Fig. 2(g). From the curves obtained in Fig. 2(g), the heat resistance index (T_{HRI}) can be directly calculated using the formula $T_{HRI} = 0.49[T_5 + 0.6(T_{30} - T_5)]$. The temperatures T_5 and T_{30} correspond to a 5% and 30% loss in weight, respectively, and are marked in Fig. 2(g) by dashed black lines. From here, the CCA@rGO/PDMS aerogels with 3.05 wt. % of CCA@rGO were found to have a T_{HRI} of 178.3 °C, which was much higher than CCA@rGO/PDMS aerogels having wt. % of 2.24 (172.4.9 °C), 2.51(173.9 °C) and 2.78 (175.7 °C). This is because more loading of CCA@rGO might enrich the interfacial intermolecular bonding network between the matrix of CCA@rGO and PDMS, this restricting molecular chain movement on heating to high temperatures and thus enhancing the thermal stability. Other literature suggesting the improvement of thermal stability due to the presence of intermolecular bonding mechanism has also been reported, such as but not limited to NFC aerogels cross-linking with diisocyanate, where the thermal stability at 500 °C was improved significantly in comparison to the un-cross-linked aerogel,[68] when the char residues of both the samples were compared.

Similar to materials such as hydrogels and aerogels, intermolecular bonding has been found to play a decisive role in increasing the thermal stability of hard materials such as composite films, too. Shang *et al.*[69] prepared polydimethylsiloxane/boron nitride nanosheets (BNNSs) based elastomer composites (PDMS/BNNS) with varying concentrations of BNNS such as 0%, 5%, 10%, 20%, and 30%. The resulting composite film contains multiple polymeric groups such as polydimethylsiloxane (H_2N–PDMS–NH_2), 1,3,5-triformylbenzene (TFB), and BNNS, the structures of which are shown in Fig. 2(h). To investigate the presence of intermolecular bonds, FTIR spectra studies were conducted as shown in Fig. 2(i). The two FTIR bands of BNNS at 812, 1370, and 3438 cm^{-1} represent out-of-plane vibration in B–N–B, in-plane vibration of the ring due to stretching, and amino (N–H) group vibrations, respectively. Furthermore, for PDMS/BNNS composites, a peak at 1650 cm^{-1}, highlighted by dashed lines, was present, representing the presence of dynamic imine bonds throughout the PDMS/BNNS composite films for all concentrations of BNNS. This polymer matrix, formed by the dynamic imine bonds in the PDMS, ensured homogenous dispersion of BNNS through the *in situ* polymerization process during preparation. As a result, strong interfacial intermolecular bonding in the matrix provided an avenue to provide favorable thermal stability of the composite film. With the increase in the content of BNNS, the thermal stability of the composites increases, as shown in Fig. 2(j). The T_5 of the pure BNNS is 392.7 °C. However, the corresponding values when PDMS, enriched in dynamic imine bonds, were added increased to 411.8 °C and 424.5 °C for the composite having 5% and 30% wt. percent of BNNS. All the PDMS/BNNS composites for BNNS wt. % between 5% and 30% showed an exceptionally high thermal stability greater than 400 °C. This enhanced thermal stability can be attributed to the higher heat stability of the BNNS, which in turn become stabilized in the polymer matrix due to the synergistic interactions between the BNNS and PDMS facilitated by the dynamic imine bonds. Besides elevated thermal stability, the imine bonds are also responsible for making the material self-healing as on cooling, the aldehyde and amino groups diffuse in the damaged interface. They re-form the imine bonds when subjected to a condensation reaction. Such self-healing and thermally stable materials can be desirable in applications related to thermal management materials. In addition to imine bonds, intermolecular hydrogen bonds can also play a prominent role in improving the thermal stability of composite films. For example, Zhang *et al.*[70] increased the cross-linking density between polyurethanes and carboxymethyl chitosan in a bio-based film. This subsequently increased the hydrogen bonding between the functional groups. The glass transition temperature also increased, implying superior thermal stability of the film.

B. Mechanical properties

Mechanical properties of various high-performance materials can also be tuned by engineering intermolecular bonding. Various strategies, such as forging intermolecular hydrogen bonds, tuning the vdW force and electrostatic interactions, and effectuating double cross-linking, for both hard (e.g., graphene-oxide nanosheets) and soft (e.g., hydrogels) materials are discussed here.

Hard materials such as graphene-oxide nanosheets, which are both mechanically strong and tough, generally two mutually exclusive properties, can be achieved by utilizing intermolecular hydrogen bond interactions between transition metallic carbides and polymers, as demonstrated by Shi *et al.*[71] Here, Ti_3AlC_2 powder was gradually stirred in a solution of water and hydrochloric acid (HCl), followed by heating, centrifugation, washing, and ultrasonication [Fig. 3(a)]. The titanium carbide (Ti_3C_2X) nanosheet (NS) dispersion thus obtained possessed abundant –OH groups and was mixed with polypropylene (PP) latex at a 30:70 ratio by weight and stirred. The mixture was then subjected to an oxygen-free drying method to obtain a powder comprised of maleic anhydride-grafted isotactic polypropylene (MA-g-PP) and titanium carbide (Ti_3C_2X). Then, the powder was melt-blended with PP granules in a roller mill to obtain the PP/MA-g-PP/Ti_3C_2TX NS nanocomposite. MA-g-PP offers a plethora of active bonding sites facilitating intermolecular hydrogen bonding, which results in nanoconfinement in the resulting nanosheet, thus improving its mechanical performance. The tensile strength of the nanocomposite increased by 35.3%, and the toughness (ductility) increased by 674.6% [Fig. 3(b)], which was considerably higher than existing PP-based nanocomposites. The reason for the superior mechanical properties was primarily due to multiple active intermolecular hydrogen

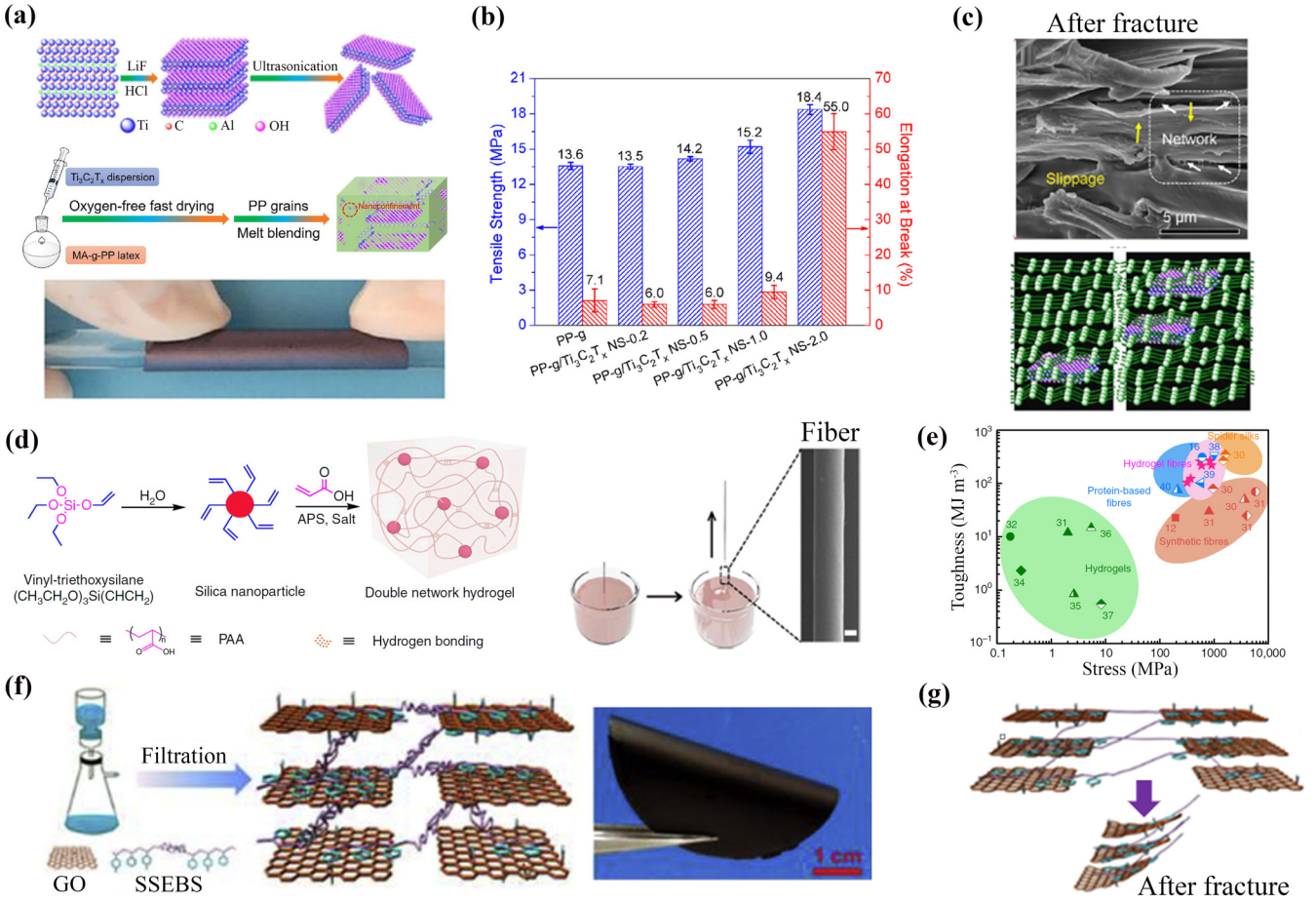

FIG. 3. Role of intermolecular bonding in elevating the mechanical properties of hard materials such as (a)–(c) nanosheets; (d) and (e) fibers, and (f) and (g) artificial nacre. (a) Schematic representation to fabricate ultrathin titanium carbide ($Ti_3C_2T_x$)/polypropylene (PP) nanocomposites (PP/MA-g-PP/$Ti_3C_2T_x$ NS) by utilizing intermolecular hydrogen bond interactions between transition metallic carbides and polymers, where MA-g-PP and NS stand for maleic anhydride-grafted isotactic polypropylene and nanosheet, respectively. (b) Mechanical performance (tensile strength in blue, elongation at break in red) of the nanocomposites for different weight content of $Ti_3C_2T_x$ and PP. (c) An SEM image (top) and model (bottom) of the multiple slippage sites of the nanocomposite on stretching. (d) Illustration showing the preparation of artificial spider silk-like fiber using vinyl-functionalized silica nanoparticles (VSNPs) to cross-link with polyacrylic acid, followed by vertical dip of a rod into the reaction mixture, concluding with quick drying by taking the rod out. (e) Plot showing the close comparison of the mechanical performance (toughness and tensile strength) of the artificial fiber with respect to other naturally occurring mechanically superior materials such as spider silk as well as synthetic fibers. (f) A schematic showing the fabrication process of an artificial nacre composed of graphene-oxide (GO) nanosheets and benzene synthesized sulfonated styrene–ethylene/butylene–styrene (SSEBS) copolymer, using a vacuum-assisted filtration process by facilitating the π–π interactions exist between the GO. The right panel shows a digital image of the nanocomposite material. (g) A molecular model showing the final stage of the proposed mechanism for fracture of this artificial nacre. (a)–(c) Reproduced with permission from Shi *et al.*, Chem. Eng. J. **399**, 125829 (2020). Copyright 2020 Elsevier. (d) and (e) From Dou *et al.*, Nat. Commun. **10**, 5293 (2019). Copyright 2019 Author(s), licensed under a Creative Commons Attribution (CC BY) license. (f) and (g) Reproduced with permission from Song *et al.*, Carbon **111**, 807 (2017). Copyright 2017 Elsevier.

bonding sites in the 3D network of Ti_3C_2X NS and the MA-g-PP. During stretching, the Ti_3C_2X NS slid relative to each other, but the active intermolecular H-bonding forged between the intermediate layers restricted the sliding. Overcoming the dense H-bonds caused multiple slippages [Fig. 3(c)] at the interface, thus dissipating a large amount of energy during the entire loading process. Thus, the failure of the MA-g-PP polymeric chains was delayed resulting in enhanced tensile strength. Moreover, the tensile stretching at higher deformation enhanced the ductility without sacrificing the tensile strength. Similar observations of intermolecular hydrogen bonding playing a predominant role in elevating strength and toughness have also been observed in other materials such as cellulose[72] and spider silk.[73]

Separate intermolecular bonding schemes utilizing a combination of electrostatic interactions and intermolecular hydrogen bonding have also been utilized so that the final developed material can possess extraordinary mechanical performance analogous to existing naturally occurring materials such as spider silk, which are

already known to possess excellent mechanical properties. This was demonstrated in the artificial spider silk-like fiber formed by a combination of ion doping followed by twisting, as reported by Dou *et al.*[74] Here, vinyl-triethoxysilane and de-ionized water were stirred to obtain vinyl-functionalized silica nanoparticles (VSNPs) [Fig. 3(d)]. Acrylic acid, ammonium persulfate, and metal salts ($ZnCl_2$, $MgCl_2$, etc.) were then added and stirred for a specific time, followed by degassing, to obtain polyacrylic acid cross-linked with VSNPs. A rod was then vertically dipped into the VSNP reaction mixture and quickly taken out, followed by drying at ambient temperature by holding at both ends, resulting in the solidified final fiber. The twisted fibers were produced by attaching both ends of the drawn non-dried fiber to a motor and a load at constant pressure. The fibers produced using this method displayed a high tensile strength (~895 MPa) and toughness (~370 MJ/m^3) [pink stars, Fig. 3(e)], better than most synthetic and protein-based fibers and closely comparable to naturally occurring mechanically superior materials such as spider silk. Here, a covalent network was formed due to the vinyl groups cross-linking in acrylic acid and/or functionalized silica nanoparticles, which was validated by NMR spectroscopy. In addition, intermolecular hydrogen bonding also formed in the active sites. Under tensile stretch, the polymeric chains elongate, and the intermolecular hydrogen bonds unzip from one site in the chain and rezip in the adjacent available site, dissipating significant energy and causing an increase in the mechanical strength and toughness. Twisting aligned the polymeric chains to a greater extent contributing to the rise in mechanical performance. Furthermore, the cross-linking facilitated by the ions from salts ($ZnCl_2$) restricted the mobility of the polymeric chains, further elevating the strength, thus making these materials suitable for multiple applications where high energy dissipation and impact absorption are required.

Utilizing vdW forces and π–π stacking interactions, in addition to other intermolecular bonding mechanisms, are also prominent in graphene-oxide (GO) based materials because GO is ideal for devising such strategies because it contains abundant oxygen-containing functional groups on its surface. Song *et al.*[75] developed an artificial nacre composed of GO nanosheets and benzene synthesized sulfonated styrene–ethylene/butylene–styrene (SSEBS) copolymer [Fig. 3(f)] using a vacuum-assisted filtration process. Here, π–π interactions exist between the GO nanosheets and benzene groups and the polystyrene chains in SSEBS. Intermolecular hydrogen bonding also exists between the –OH and –COOH groups of the GO nanosheets with the sulfonic groups in SSEBS. This caused the failure mechanism to progress in the proposed steps starting with the deformation of EB chains in SSEBS between the inter-layer spaces occupied by the GO NS. This was followed by further elongation of the chains till failure along with some proportion of partially slipped GO NS [Fig. 3(g)]. The combined synergistic intermolecular bonding mechanisms comprised of H-bonds and π–π stacking interactions thus increased the interfacial stress transfer efficiency leading to high energy dissipation, which caused toughness (15.3 MJ/m^3) significantly higher than natural nacre and many other morphologically similar GO-based nanocomposites. Modeling-based studies predicting the mechanical properties as a function of graphene interlayer cross-links have also been performed[76] to aid in the mechanistic design of GO-based sheets. Such models can predict the location of the maximum strain (e.g., at the edges) and how adjusting the cross-links through successful intermolecular bonding strategies (hydrogen, vdW, metal ions, etc.) can help improve the mechanical performance of the nanocomposite.

Another method of tuning intermolecular bonds to obtain enhanced mechanical properties, e.g., higher strength and toughness, can also be realized by engineering the noncovalent interfaces of hierarchical material architecture.[77,78] Generally, this design strategy is inspired by the architecture of natural biomaterials, such as wood, bone, conch shell, and nacre.[79] These natural biomaterials consist of building blocks that span across several length scales. The mechanics of these biomaterials is largely dependent on the interfaces among the building blocks. Insight from understanding the mechanics of such biomaterials can help design advanced materials with remarkable mechanical performance.[80] For example, natural nacre is known to have exceptional mechanical properties.[81–83] Inspired by natural nacre, Zeng *et al.*[84] used a vacuum-assisted self-assembly method to fabricate artificial nacre-like papers comprised of noncovalent functionalized boron nitride nanosheets (NF-BNNSs) and polyvinyl alcohol (PVA). In the ordered "brick-and-mortar" material structure analogous to natural nacre, the long PVA molecular chains can tune the noncovalent interfaces by linking the NF-BNNSs through intermolecular hydrogen bonds. The resulting artificial nacre-like paper demonstrated outstanding mechanical strength (125.2 MPa, similar to natural nacre) and toughness (2.37 $MJ\,m^{-3}$) 30% better than natural nacre. Theoretical studies on nacre-like bio-inspired composites by optimizing material compositions (e.g., volume fraction, aspect ratio, and offset ratio) and resolving the conflicts among mechanical properties have also been demonstrated.[85] A combination of atomistic modeling and experimental investigation[86] also demonstrated superior strength and toughness in disc-shaped material molds made of silica-polymer composites. The inorganic silica network could covalently bond with the polymer [polytetrahydrofuran (PTHF)] chains. This was because of the molecular structure of PTHF and the presence of other organic silane coupling agents. The intermolecular bonding thus formed was crucial in increasing the strength of the hybrid by ~321% % (from 0.32 to 1.35 MPa) and toughness by 82% (from 120 to 219 kPa). The above research efforts epitomize the effectiveness of designing and fabricating synthetic materials with desirable mechanical performance by tuning the noncovalent interfaces.

Apart from hard materials, soft materials such as hydrogels can also be fabricated by effective intermolecular bonding strategies. Hydrogels[19,87] are a representative class of materials possessing a complex, three-dimensional network of polymeric chains with water occupying the molecular voids in between. Here, the molecular properties of water are retained as the polymer network mesh is much larger than individual molecules of water. The hydrophilic functional groups of the polymeric framework make it swell, a distinctive feature of hydrogels, and enable this material to have a high water retention capacity. But the chemically induced cross-links among the constituent polymers restrict the dissolution of hydrogels in water. From a mechanistic standpoint, the brittle and tightly linked part of the network is primarily responsible for energy dissipation. In contrast, the ductile and loosely linked part

helps conserve elasticity. Different novel cross-linking strategies are thus considered to render magnified mechanical stability to the hydrogel network,[88,89] which has benefits in multiple applications. In one such study, Gong *et al.*[61] reported a general method to combine different hydrophilic polymers to obtain a double-network (DN) hydrogel with high mechanical strength (tensile strength up to 17.2 MPa, fracture strain up to 98%). For example, the first network of PAMPS and PAA was synthesized from methypropanesulfonic acid and a cross-linking agent (methylenebisacrylamide), followed by the synthesis of the second network in the presence of the first.[90] This investigation demonstrated that for two networks of polymers entangled with each other in a hydrogel, different parameters such as the molar ratio of the first network to the second, the cross-linking density of the first (high cross-linking) concerning the second (loose cross-linking) network are of crucial importance to obtain a high mechanical strength hydrogel.

For this DN hydrogel[61] comprising of a short-chain network of poly(1-acrylanmido-2-methylpropane sulfonic acid) (PAMPS) and a long-chain network of polyacrylamide (PAAM) polymers, fatigue behavior was also studied by Zhang *et al.*[91] During stretching, the short-chain network ruptures and dissipates energy. In contrast, the long-chain network contributed to the retention of the hydrogel elasticity for both types of prepared samples, cut and uncut [Fig. 4(a)]. On application of a cycle of loading and unloading in the PAMPS/PAAM network, the PAMPS network broke. Still, the PAAM network was preserved [Fig. 4(b)]. Cyclic load applied on uncut samples to check the stress-stretch curves revealed that the internal damage could accumulate through thousands of cycles before final failure. On application of cyclic loading on cut samples to study the fatigue crack propagation, it was observed that the crack travels cycle-wise when a stretch amplitude beyond a certain value was applied. The threshold for energy release rate, indicating when the crack starts propagating, was observed to be higher ($\sim$400 J/m^2) in PAAM networks having low-density cross-linkers and lower ($\sim$200 J/m^2) in PAAM networks having high-density cross-linkers, which was validated using the Lake–Thomas model. Such a study of fatigue behavior is essential for using hydrogels in applications where a large load needs to be sustained.

Novel design strategies to fabricate DN hydrogels with high self-recovery and improved fatigue resistance have also been demonstrated by incorporating ions in the second network, as reported by Chen *et al.*[92] Here, a hybrid DN gel was fabricated comprising physically cross-linked (via hydrogen bonding) Agar gel as the first network and chemically–physically cross-linked copolymer of acrylamide and acrylic acid (PAMAAc) gel as the second network. The hybrid DN gel was soaked in the Fe^{3+} solution at optimal conditions, and utilizing the strong intermolecular coordination bonding, Agar/PAMAAc-Fe^{3+} DN gels were obtained [Fig. 4(c)]. The mechanical properties of the obtained hybrid DN gel (strength $\sim$ 1.55 MPa) were found to be much superior [Fig. 4(d), top panel] than the gel without any ion intercalation or the gel that did not possess double network [PAMAAc-Fe^{3+} gel, top panel of Fig. 4(d)], emphasizing on the role of the coordination interactions to improve the mechanical properties in DN hydrogels. The hybrid DN gel even self-recovered almost 50% of its toughness around 1 min after removal of loading [Fig. 4(d), bottom panel], which can be attributed to the synergistic effect of intermolecular bonding (hydrogen bonds in the first network and coordination bonds in the second network), causing immense energy dissipation internally and thus delaying the fracture. Furthermore, manipulation of the second network content (AAc varied from 1 to 20 mol. %) of the DN gel also demonstrated even higher mechanical strength ($\sim$8 MPa) and was subjected to six loading cycles; the hysteresis loops remained almost the same during the last four cycles. The latter phenomenon demonstrates its superior fatigue resistance due to Fe^{3+} coordination bonding offering a higher withstanding capacity of larger stress, paving the path for applying these freely shapeable [Fig. 4(d), side panel] double-network hydrogels in the development of strong and tough, shape-shifting next-generation soft materials.

Separate studies modifying the DN design strategies and forming a triple-network (TN) supermacroporous hydrogel in the same manner by using the DN network [Fig. 4(e)] as the precursor have also been demonstrated,[93] which had a much higher compressive modulus [Fig. 4(f)] than double-network (DN) or single-network (SN) hydrogels. Hydrogels having mesoscale networks containing constituent structures at different length scales (e.g., ionic bonds at the $\sim$0.1 nm scale, transient polymer network at $\sim$1 nm scale, permanent chemically cross-linked network at the $\sim$10 nm scale, bicontinuous hard/soft phase at $\sim$100 nm scale) have also been observed to be tough, self-healing, and fatigue resistance as demonstrated by Li *et al.*[94] with detailed analysis on factors determining the rate (slow/fast) of crack propagation. Similar mechanistic analysis on the suppression of crack advance in other mesoscale network hydrogels has also been reported.[95,96] Apart from this, numerous modeling studies including, but not limited to, enriching the design of DN hydrogels with a focus on constitutive models[97] revealing the mechanism of damage and also finite element models[98] studying the deformation regime near the crack tip of chemically and physically cross-linked PVA-based hydrogel are also reported, which vividly elucidates the importance of intermolecular bonding on these novel soft materials.

Other soft materials, such as aerogels, have also exhibited superior mechanical performance due to incorporation of intermolecular bonding. Aerogels are materials composed of a complex interconnected network of fibers confined together by diverse intermolecular bonding mechanisms. Aerogels are obtained from hydrogel as a starting material, then subjected to a series of physical/chemical treatments. For example, polyvinyl alcohol (PVA), phytic acid (PA), and montmorillonite (MMT) was used to fabricate an aerogel utilizing both physical and chemical cross-linking design strategies.[99] PVA, PA, and MMT were mixed in an aqueous suspension where the rich –OH groups in each of them were responsible for forming hydrogen bonding and thus enabling physical cross-linking [Fig. 4(g)]. Then, the solution was freeze-dried by using a vacuum oven to obtain the final aerogel. The freeze-drying process enabled the esterification of PVA and PA, resulting in the chemical cross-linking [Fig. 4(g)]. The resulting double-network aerogel was ultralight (0.078–0.103 gm/cm^3) and possessed an ultrahigh compressive modulus ($\sim$41.9 MPa) [Fig. 4(h)] when compared with similar single and double cross-linked aerogels. The ultralow density resulted in the aerogel standing on the flower petals lightly [Fig. 5(h)], while the ultra-strong bonding leads to the ultrahigh resistance from the crushing of a car ($\sim$1520 kg) and bicycle tires ($\sim$75 kg), as shown by SEM imaging in Fig. 5(i). It should be noted

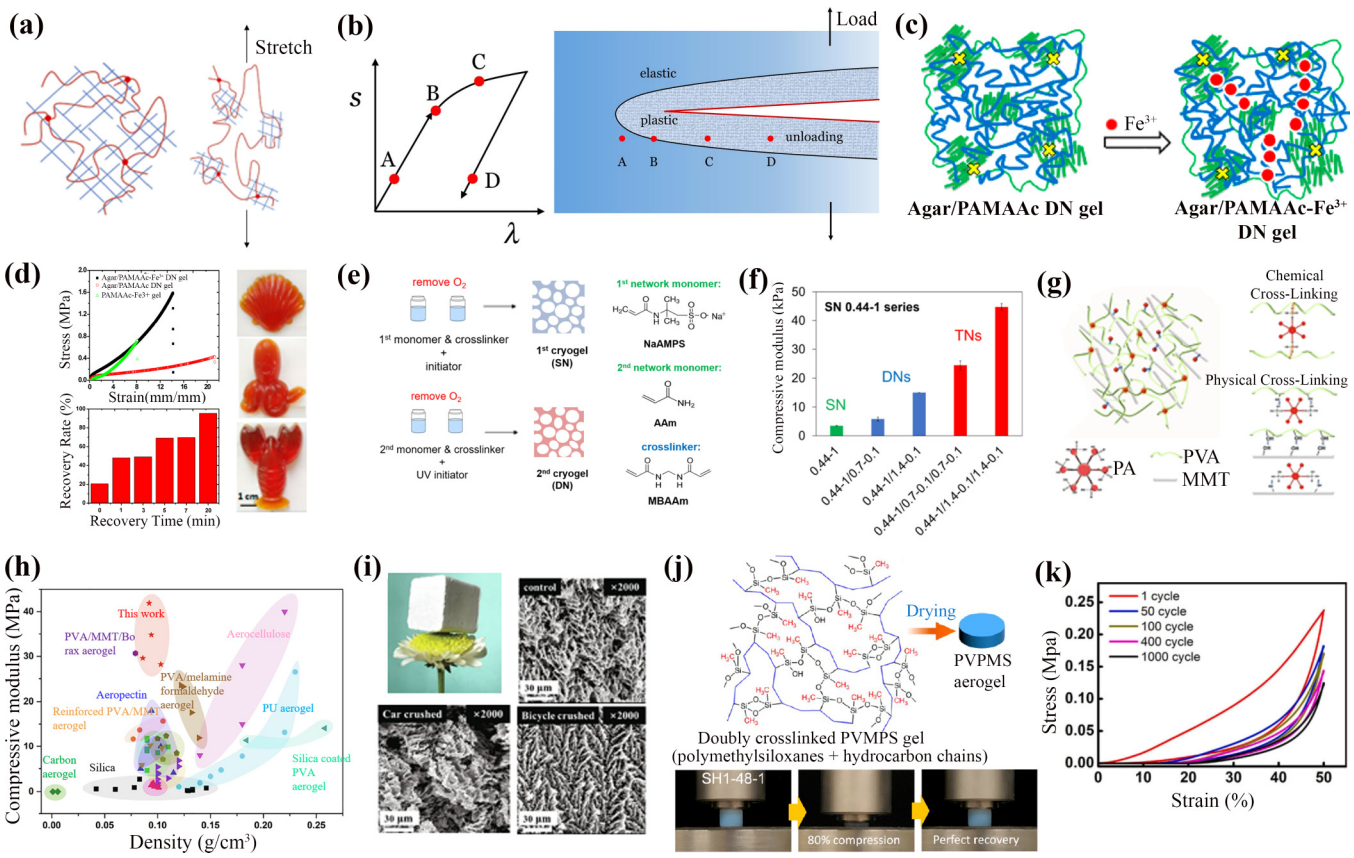

FIG. 4. The role of intermolecular bonding in elevating the mechanical properties of soft materials such as (a)–(f) hydrogels and (g)-(k) aerogels. (a) Schematic of a double-network (DN) hydrogel, a short-chain network of PAMPS, and a long-chain network of PAAM polymers. (b) Typical loading/unloading cycle of the hydrogel during stretching (left panel). Fatigue crack propagation on the application of cyclic loading (right panel). (c) Schematic of a hybrid DN gel composed of Agar gel in the first network and a chemically cross-linked copolymer of acrylamide and acrylic acid (PAMAAc) gel in the second network, soaked in Fe^{3+} solution. (d) Stress–strain plots show the superior mechanical strength of the hybrid DN gel (top panel) and the self-recovery characteristics (bottom panel). The side panel shows the digital images of the easily shapeable DN gel. (e) A schematic of the two-step process to fabricate DN cryogels. (f) Comparison of the compressive modulus values for the triple-network (TN) gel with the DN and single-network (SN) gels. (g) A schematic of the two-step process to fabricate a double-network aerogel using physical and chemical cross-linking of polyvinyl alcohol (PVA), phytic acid (PA), and montmorillonite (MMT). (h) Comparison of the ultra-high compressive modulus (MPa) of the aerogel (red star labeled "This work") in this work with other similar single and double-network aerogels. (i) Top left image shows the ultra-light double-network aerogel resting on a flower. The top right, bottom left, and bottom right are the SEM images after the aerogel is crushed under control, car and bicycle, respectively. (j) Schematic (top) of an aerogel structure comprised of polyvinylpolymethylsiloxane (PVPMS), prepared through a facile synthesis route involving radical polymerization and hydrolytic polycondensation. The bottom panel shows image evidence of the remarkable self-recovery characteristics of the aerogel. (k) Stress–strain plots of a GO-based aerogel infested with cobalt ions, developed by facilitating coordination bond interactions (chemical cross-link) along with hydrogen bonding (physical cross-link) under multiple (till 1000) loading cycles. (a) and (b) Reproduced with permission from Zhang *et al.*, Eng. Fracture Mech. **187**, 74 (2018). Copyright 2018 Elsevier. (c) and (d) Reproduced with permission from Chen *et al.*, Chem. Mater. **28**, 5710 (2016). Copyright 2016 American Chemical Society. (e) and (f) Reproduced with permission from Sedlačík *et al.*, Chem. Mater. **32**, 8576 (2020). Copyright 2020 American Chemical Society. (g)–(i) Reproduced with permission from Shi *et al.*, Chem. Eng. J. **399**, 125829 (2020). Copyright 2020 Elsevier. (j) Reproduced with permission from Zu *et al.*, ACS Nano **12**, 521 (2018). Copyright 2018 American Chemical Society. (k) Reproduced with permission from Zhang *et al.*, Chem. Eng. J. **381**, 122784 (2020). Copyright 2020 Elsevier.

that optimal proportion of the elements in the double network is of prime importance to extract the best mechanical performance. A greater proportion of PA disrupted its ability to engage in excessive cross-linking, thus distorting the stable double cross-linked hydrogel network.

Other design techniques effectuating enhanced intermolecular bonding by implementing double cross-linking have also been demonstrated by altering the modes of physical and chemical treatments. For example, polyvinylpolymethylsiloxane (PVPMS) aerogel was prepared through a facile synthesis route[100] involving radical polymerization and hydrolytic polycondensation [Fig. 4(j)], which enabled the double chemical cross-linking between polymethylsiloxanes and hydrocarbon chains, followed by drying using different methods such as ambient pressure drying or solar conduction

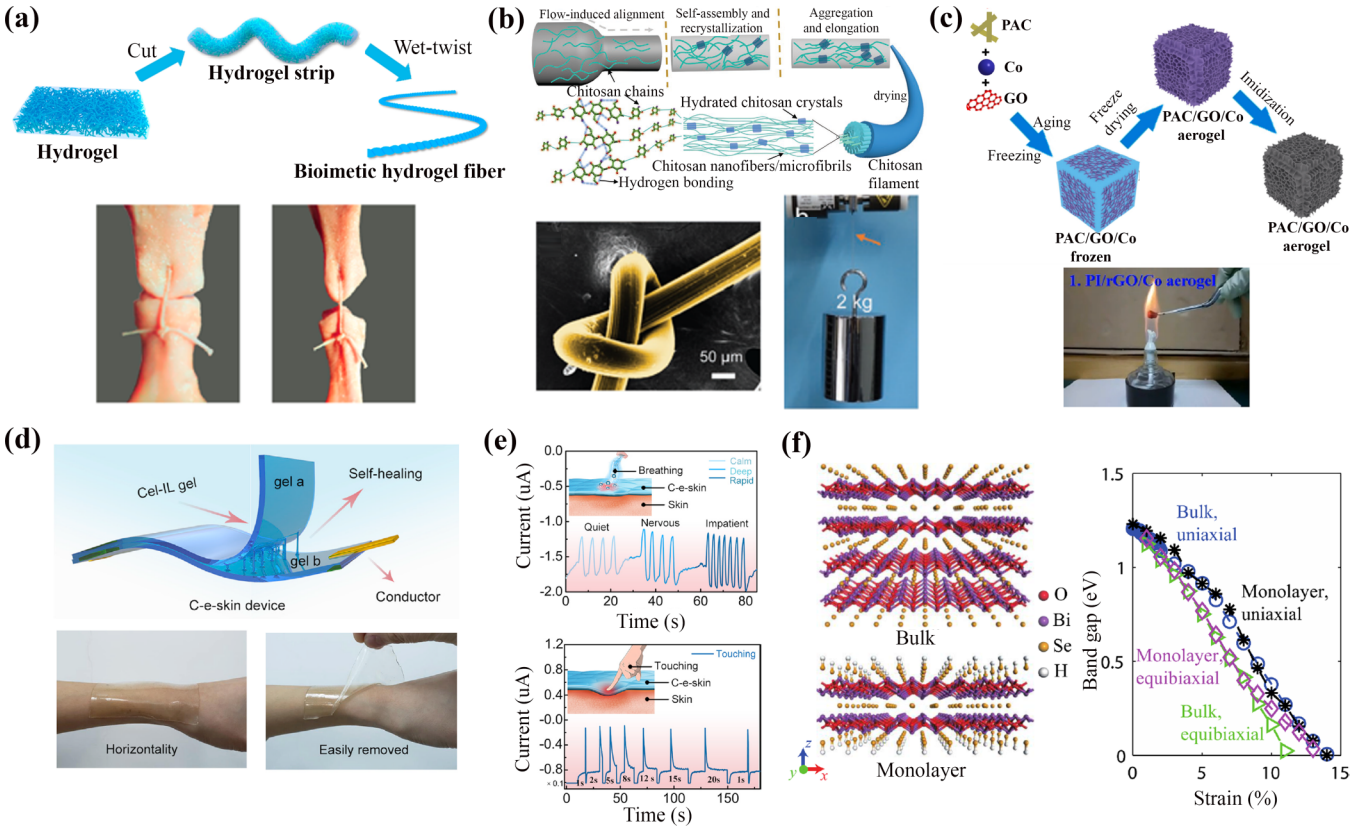

FIG. 5. A few selected applications fostered by the enhanced material properties when the material structure is subjected to a greater degree of intermolecular bonding. (a) Biomimetic devices, (b) Smart textiles, (c) Structural and thermal insulation materials, (d) and (e) Artificial skins, and (f) Semiconductor devices. (a) Reproduced with permission from Guan *et al.*, ACS Nano **15**, 7889 (2021). Copyright 2021 American Chemical Society. (b) Reproduced with permission from Chen *et al.*, Adv. Funct. Mater. 2104368 (2021). Copyright 2021 Wiley-VCH.[24] (c) Reproduced with permission from Chem. Eng. J. **381**, 122784 (2020). Copyright 2020 Elsevier.[101] (d) and (e) Reproduced with permission from Matter **2**, 390–403 (2020). Copyright 2020 CellPress.[123] (f) Reproduced with permission from J. Mech. Phys. Solids. 104626 (2021). Copyright 2021 Elsevier.[124]

drying. The transparent aerogel displayed extraordinary compression flexibility [till 80% strain without fracture with recovery to the original shape, as shown in Fig. 4(j), bottom panel] and superior bending flexibility. These exquisite mechanical properties were primarily due to the hydrogen bonds in the $-CH_3OH$ groups of the polymethylsiloxane skeleton, which aided in the recovery when compressed or bent, as well as the chemical cross-linking between the polymethylsiloxane skeleton and hydrocarbon chains, which increased the deformability under compression. This work shows significant progress in double cross-linked aerogels, which can be used in insulator applications in the near future. Apart from the above outstanding mechanical properties, the aerogel also presents us the high fatigue resistances. Zhang *et al.*[101] demonstrated a double cross-linked hydrogel facilitating the coordination bond interactions (chemical cross-link) along with hydrogen bonding (physical cross-link). Here, hydrogen bonds formed between GO nanosheets, and coordination interactions inflicted by cobalt ions were applied in the resulting GO-polymer-based aerogel. The final aerogel possessed a high (0.506 MPa) compression modulus, 43% improvement of tensile modulus, and high fatigue resistances lasting over 1000 cycles [Fig. 4(k)]. Such aerogels fabricated using relatively green, cheap, non-chemically toxic methods could be used as an insulating material in multiple applications proving the effectiveness of a successful intermolecular bonding scheme in aerogel-like materials. Aerogels fabricated using such innovative mechanistic design strategies described above have already been found to be useful in multiple applications related to super elasticity, thermal insulation,[102–105] heat stability,[101] phase change materials,[106] biomedical industry,[107] wearable sensors,[105,108–111] contaminant filters,[62,112,113] some of which will be discussed in Sec. IV.

IV. APPLICATIONS

The enhanced properties fostered by engineering intermolecular bonding lead to multiple applications crucial to instigating the materials science community in designing next-generation

materials.[114,115] Some of those applications are categorized here primarily based on thermal and mechanical properties, which have been observed to improve significantly due to manipulation of the intermolecular bonding as reviewed above. Other applications based on properties related to electronics, sensing, optics, and biomedical uses are also briefly reviewed to demonstrate the versatility in materials development due to maneuvering intermolecular bonds.

Facilitating intermolecular bonding to tune thermal properties has been done in many materials, such as, but not limited to, $Ti_3C_3T_x$ MXene/poly (vinyl alcohol) (PVA) composites.[116] Here, the incorporation of PVA, forged hydrogen bonds between the MXene and PVA due to the presence of hydroxyl groups in the PVA and Ti–O bonds, as confirmed by spectroscopy. Thereby, the thermal stability significantly improved, as indicated by the reduction of the thermal coefficient from −0.06271 to −0.03357 cm^{-1}/K. Furthermore, the thermal conductivity of the PVA based composite was higher (∼47.8 W/mK) than many metals and most two-dimensional materials. Such nanocomposites may have novel future uses in battery and thermoelectric devices. Soft materials like hydrogels based on polymers, such as NFCs, contain spatially dense hydrogen bonding networks between the NFCs and water,[89] and can be used as a raw material for biomimetic devices [Fig. 5(a)]. When a double-network hydrogel is fabricated based on NFCs and CNTs using wood as substrate, the NFC/CNT layer protected the wood substrate by localizing heat, thus acting as an effective thermal insulation layer, which can be considered a future candidate for water purification, ionic conductors, and biomedical devices. Other soft materials such as double cross-linked aerogels[105] based on polyvinylpolydimethylsiloxane show low thermal conductivities (∼16.2 W/K), which are much lower than standard insulating materials such as stationary air (26 W/K), nanocellulose and chitosan aerogels (22–30 W/K), polyurethane (20–50 W/K), mineral wool (35–80 W/K), etc., thus demonstrating their extraordinary thermal insulation performance.

Intermolecular bonding, if tuned appropriately, can result in mechanically strong and tough materials replicating natural materials. For example, Liao *et al.*[117] demonstrated strong (∼1236 MPa) and tough (∼137 J/gm) fibers with mechanical properties comparable to spider silk from yarn by electrospinning, stretching, and cross-linking using a minor amount of poly (ethylene glycol) bisazene. Techniques such as these, when applied to commercial polymers may be an effective method to design fibers with possible applications in satellite technology, biomedicine, and automobiles. A simple but sustainable two-step drawing process[24] using a chitosan and KOH/urea aqueous solution brought the inherent smaller fibers in closer proximity because of flow-induced alignment, thus increasing the spatial intermolecular hydrogen bond density and resulting in super stiff (∼44.7 GPa) and strong (∼878 MPa) chitosan filaments which could demonstrate vital applications as smart textiles such as lifting heavy weights [Fig. 5(b)]. A combination of chemical cross-linking and intermolecular hydrogen bonding has also been exhibited to demonstrate high strength (13.7 MPa), toughness (11.8 MJ/m^3), and strain at break (91.8%) in hyperbranched polyester doped soy protein films[25] which could prove to be of great use in recyclable tissue engineering and packaging applications. This proves how various effective intermolecular bonding strategies can be extended for the bottoms-up design of multiple strong and tough materials with targeted properties, paving the way for application in many practical applications needing mechanically superior materials. Soft materials such as double cross-linked aerogel based on polyimide/reduced graphene-oxide/cobalt have also been demonstrated[101] to possess superior mechanical properties such as high modulus and high fatigue resistance which can prove very useful in applications like structural materials in buildings and pipelines as well as for thermal insulation materials [Fig. 5(c)]. Polyimide (PI) based aerogels[118] using amino-functionalized carbon nanotubes as cross-linkers have been found to demonstrate mechanically strong (∼2 MPa) aerogel materials where the compression modulus increased from 4.2 MPa in pristine PI based aerogels to ∼47.3 MPa when intermolecular bonding strategy of cross-linking was adopted. The drastic increase of compression modulus aerogel by over 1100%, along with its high strength, indicates its applicability in lightweight, high-performance applications in the aerospace sector where strong materials providing superior thermal insulation are needed. Other soft materials such as cross-linked hydrogel inspired from natural substances such as mussels are already being manufactured with tunable mechanical properties such as stress, strain, Young's modulus, and toughness, which could be very useful in wearable sensor applications used in smart textiles.[119] Cross-linked hydrogels, when infested with different ions,[120] have also been observed to remarkably increase their mechanical properties (strength from ∼50 kPa to ∼15 MPa; toughness from ∼ 0.0167 to ∼150 MJ/m^3; elongation from ∼300% to ∼2100%; modulus from ∼24 to ∼140 kPa), manifesting the suitability of its usage in flexible electronics. Double-network hydrogels have also found their applicability in many useful and life-saving biomedical applications to cure cancer cells.[121]

Tuning intermolecular bonds can also accelerate the enhancement of other lucrative properties of materials along with mechanical properties. Hydrogels can be used in artificial skins,[122] human–machine interaction devices such as touchpads, and triboelectric generators to convert mechanical movement to electric current, widely used in pressure sensing electronics. Dynamic methylimidazolium chloride-based gels[123] [Fig. 5(d)] have also been designed to have tunable topological networks, reversible properties related to toughness, and electric conductivity along with adhesive and self-healing properties, which may find their applications in artificial skins located in smart devices to detect the style of breathing and touch [Fig. 5(e)]. Bi_2O_2Se as the layered structure is stacked through the electrostatic interaction [Fig. 5(f)]. Recent research reveals that strain engineering can be utilized to modify this interlayer interaction and thus results in the conversion from semiconductivity to metallicity.[124] All this enormous attention suitably proves the potential of intermolecular bond engineering to significantly alter various physical properties such as thermal stability and mechanics and emphasizes the urgent need to pursue research and development in this direction.

V. CHALLENGES AND FUTURE PERSPECTIVES

Despite the prominent interest in recent years in engineering intermolecular bonds and fabricating novel materials with superior physical properties, a few challenges related to intermolecular

bonding strategies need to be addressed to foster research using these approaches. Some of the notable challenges posing as obstacles in this domain are discussed in this section.

For crystalline structures, it is a standard practice to compute phonon dispersion curves[125,126] to identify whether the in-plane or out-of-plane vibrations of atoms are the dominant factors influencing thermal conductivity. A shift in the phonon spectra correlates with an increase or decrease in energy of the phonons in the bulk composite, which is directly related to the increase or decrease of the thermal conductivity of the material. However, to the best of our knowledge, this method is yet to be applied specifically to intermolecular bonded molecular regions, which could shed light on the fundamental reason for how intermolecular interactions lead to enhancement or weakening of the overall thermal conductivity values. Some studies[127] on strong/weak intermolecular hydrogen bond interactions between small, large, or continuous polymer blends affecting the thermal transport pathway could serve as a starting point in pursuing this research area which may enable obtaining targeted thermal conductivities. The molecular origin of various kinds of intermolecular interactions, bridging the bonding between molecules, affecting the phonon transport and thus the thermal conductivity of these structures is largely unknown, which, if possible, could help guide the thermal management of multiple beneficial devices.

The simultaneous improvement in strength and toughness is typically absent for traditional materials. But such a challenge has been addressed in some materials such as MXenes,[128] metal oxides,[129,130] cellulose,[18] dendrite composites,[131–133] and carbon-based composites[130,134] by adopting different intermolecular bonding strategies. Applications of these strategies alter the material nano/micro-structure through different processes such as self-assembly, the introduction of anisotropy and/or chemically modified molecules or functional groups. These processes, along with the modifications they induce on the final mechanical properties, are well-documented. However, there is a lack of standardized experimental evidence that elucidates the mechanism of enhancement or weakening of the mechanical properties due to implementing these strategies. For example, an accurate, stepwise representation of a generalized failure mechanism in the resulting mechanically superior materials is still elusive. Furthermore, intercalated ions and molecules influence the enhancement of the mechanical properties, such as cellulose intercalated with water molecules[135] or polymers/graphene intercalated with ions.[136] Experimental results on increased mechanical strength by increasing the proportion of ions/molecules have also been demonstrated.[137] But there is still no research, to the best of our knowledge, which delineates the mechanism illustrating how this intercalation process evolves. Such knowledge may help identify the parameters that govern what ratio of intercalated ions/molecules best optimizes the mechanical properties. Without a proper understanding of a generalized mechanism, different intermolecular bonding techniques applied by various research groups lead to materials with diverse final morphology. Such practice might make that specific material suitable for selected use but prohibits extending that study to multifaceted applications.

One of the unique features of successful intermolecular bonding is the development of large failure strain and remarkable thermal stability, as already discussed before. As a result, applications of such materials may become feasible in extreme environments caused by external factors such as, but not limited to, high temperature, pressure, or humidity. For example, a polyimide-based sensor,[138] comprised of ether and anhydride, could survive a wide spectrum of temperatures ranging from −150 to 300 °C and withstanding high deformations. It might make its applications possible for recording temperature in non-contact mode, a desirable feature for wireless temperature sensing. Similar other representative studies exist which elucidate how to achieve superlative electronic properties in extreme environments (e.g., flame, high pressure, and humidity).[139–141] But the detailed process describing how the intermolecular bonding evolves in extreme environments and modifies the electronic properties is still unknown. Shedding light on this topic might be a great perspective for future researchers.

Another challenge that researchers should address is the large gap that exists in scaling up the bottoms-up design of tuning the intermolecular bonds toward bulk materials properties. Fundamental building blocks often have superior mechanical properties that are orders of magnitude higher than their bulk counterpart. For example, isolated crystalline cellulose nanocrystals may have high strength (1.6–7.7 GPa)[142,143] and stiffness (150 GPa),[144–146] but natural wood that primarily contains cellulose has much lower strength (100 MPa) and stiffness (few GPa).[147] Efforts are ongoing to correlate the molecular properties with the bulk for materials such as, but not limited to, biomimetic polymers[148] and gel.[149] In these studies, the force spectroscopy between functional groups has been demonstrated to agree reasonably well with the bulk mechanical properties. However, these strategies are still far from being standardized. Furthermore, developing a prototype material in the lab often focuses on obtaining superior physical properties by overlooking other important aspects, such as a robust life cycle analysis of the entire process and the wastage of chemicals or water. But neglecting these aspects might hinder the industrial-scale fabrication of these advanced materials.

Another significant hurdle that needs to be overcome is scaling up the computational modeling framework and predicting the properties of advanced materials.[150] The nanoscale phenomenon becomes negligible at the continuum level, whereas continuum mechanics cannot consider the beneficial effects of microscale and molecular levels. A robust theoretical framework incorporating multiscale mechanics and cross-scale modeling is needed to capture the mechanical properties dominated by material structure and composition in advanced materials. There exist constraints to developing such a framework mainly because of the limitations on the existing computational capabilities.[151,152]

Novel computational techniques such as machine learning (ML) aided materials discovery[153–160] might provide another avenue to accelerate materials design by various intermolecular bonding strategies. For example, hydrogen bond donor and acceptor strengths[161] in chloroform (CCl_4) were determined using ML methods with values quite close to experiments, typically done using infrared spectroscopy techniques. This can prove to be a fast predictor by substituting experiments and avoiding repeated trial and error that wet lab experimental procedures typically entail, as well as significantly reducing the time taken for manually identifying useful hydrogen bond strength information after navigating

previous literature. However, the hydrogen bond energy databases to train the ML models need to be expanded significantly to apply to other molecules beyond CCl_4. Furthermore, unlocking the nature of chemical bonding between different molecules by evaluating how different molecules bind with each other could help realize how to control the strength of bonds by ML-based models. Some research on this domain has been done by applying the Bayesian learning-based model[162] to decipher how catalysts bind with different intermediate molecules leading to efficient catalytic processes and may have the potential to be extended to separate processes. There exist fertile opportunities for new materials development by tuning intermolecular bonds that call for collaborations among interdisciplinary researchers. Such collaborations will help in exploring facile and unconventional strategies of programming materials properties by engineering intermolecular bonding. The rational materials design scheme obtained will accelerate the discovery of new functional materials with the potential to address rising global challenges, such as reducing energy consumption and diminishing carbon footprint.

ACKNOWLEDGMENTS

The authors acknowledge the support of the U.S. National Science Foundation (Grants No.: 1362256 and 1936452) and the University of Maryland supercomputing resources (http://hpcc.umd.edu).

AUTHOR DECLARATIONS

Conflict of Interest

The authors hereby declare no conflict of interest.

Author Contributions

Upamanyu Ray: Investigation (equal); Visualization (lead); Writing – original draft (equal). **Zhenqian Pang:** Investigation (equal); Writing – original draft (equal). **Teng Li:** Conceptualization (lead); Funding acquisition (lead); Investigation (lead); Project administration (lead); Resources (lead); Supervision (lead); Writing – original draft (equal); Writing – review & editing (lead).

DATA AVAILABILITY

Data sharing is not applicable to this article as no new data were created or analyzed in this study.

REFERENCES

[1]K. Lu, L. Lu, and S. Suresh, Science **324**, 349 (2009).
[2]L. Lu, X. Chen, X. Huang, and K. Lu, Science **323**, 607 (2009).
[3]T. Zhu and J. Li, Prog. Mater. Sci. **55**, 710 (2010).
[4]L. Lu, Y. Shen, X. Chen, L. Qian, and K. Lu, Science **304**, 422 (2004).
[5]R. O. Ritchie, Nat. Mater. **10**, 817 (2011).
[6]A. G. Evans, J. Am. Ceram. Soc. **73**, 187 (1990).
[7]D. C. Hofmann, J. Suh, A. Wiest, G. Duan, M. Lind, M. D. Demetriou, and W. L. Johnson, Nature **451**, 1085 (2008).
[8]M. D. Demetriou, M. E. Launey, G. Garrett, J. P. Schramm, D. C. Hofmann, W. L. Johnson, and R. O. Ritchie, Nat. Mater. **10**, 123 (2011).
[9]B. M. E. Launey and R. O. Ritchie, Adv. Mater. **21**, 2103 (2009).
[10]X. Zhao, X. Chen, H. Yuk, S. Lin, X. Liu, and G. Parada, Chem. Rev. **121**, 4309 (2021).
[11]Y. Yanagisawa, Y. Nan, K. Okuro, and T. Aida, Science **359**, 72 (2018).
[12]P. I. Nagy, Int. J. Mol. Sci. **15**, 19562–19633 (2014).
[13]N. Ramasubbu, R. Parthasarathy, and P. Murray-Rust, J. Am. Chem. Soc. **108**, 4308 (1986).
[14]U. Ray, Z. Pang, and T. Li, Cellulose **28**, 3359–3372 (2021).
[15]U. Ray, S. Zhu, Z. Pang, and T. Li, Adv. Mater. **33**, 2002504 (2021).
[16]T. Li, Extreme Mech. Lett. **42**, 101107 (2021).
[17]Q. Chen, B. Chen, S. Jing, Y. Liu, and T. Li, Extreme Mech. Lett. **56**, 101865 (2022).
[18]H. Zhu, S. Zhu, Z. Jia, S. Parvinian, Y. Li, O. Vaaland, L. Hu, and T. Li, Proc. Natl. Acad. Sci. U.S.A. **112**, 8971 (2015).
[19]J. Kim, G. Zhang, M. Shi, and Z. Suo, Science **374**, 212 (2021).
[20]B. C. Gibb, Nat. Chem. **12**, 665 (2020).
[21]J. Zhang, P. Chen, B. Yuan, W. Ji, Z. Cheng, and X. Qiu, Science **342**, 611 (2013).
[22]C. Fonseca Guerra, F. M. Bickelhaupt, J. G. Snijders, and E. J. Baerends, Chem. Eur. J. **5**, 3581 (1999).
[23]C. Fonseca Guerra and F. M. Bickelhaupt, Angew. Chem. Int. Ed. **38**, 2942 (1999).
[24]Y. Chen, Q. Zhang, Y. Zhong, P. Wei, X. Yu, J. Huang, and J. Cai, Adv. Funct. Mater. **31**, 2104368 (2021).
[25]W. Gu, X. Liu, Q. Gao, S. Gong, J. Li, and S. Q. Shi, ACS Sustain. Chem. Eng. **8**, 7680 (2020).
[26]K. Mizuno, Y. Miyashita, Y. Shindo, and H. Ogawa, J. Phys. Chem. **99**, 3225 (1995).
[27]J. P. M. Lommerse, S. L. Price, and R. Taylor, J. Comput. Chem. **18**, 757 (1997).
[28]A. Vila, R. A. Mosquera, and J. M. Hermida-Ramón, J. Mol. Struct. Theochem. **541**, 149 (2001).
[29]D. Ye, X. Lei, T. Li, Q. Cheng, C. Chang, L. Hu, and L. Zhang, ACS Nano **13**, 4843 (2019).
[30]Z. Fang, H. Zhu, Y. Yuan, D. Ha, S. Zhu, C. Preston, J. Huang, and L. Hu, Nano Lett. **14**, 765-773 (2014).
[31]M. Henriksson, L. A. Berglund, P. Isaksson, T. Lindström, and T. Nishino, Biomacromolecules **9**, 1579 (2008).
[32]E. Navarro, L. Franco, J. A. Subirana, and J. Puiggalí, Macromolecules **28**, 8742 (1995).
[33]R. Xu, Y. Qiu, S. Tang, C. Yang, Y. Dai, D. Zhang, Y. Gao, K. Gao, L. Luo, and X. Liu, Macromol. Mater. Eng. **306**, 2000814 (2021).
[34]G. R. Bhimanapati, Z. Lin, V. Meunier, Y. Jung, J. Cha, S. Das, D. Xiao, Y. Son, M. S. Strano, V. R. Cooper, L. Liang, S. G. Louie, E. Ringe, W. Zhou, S. S. Kim, R. R. Naik, B. G. Sumpter, H. Terrones, F. Xia, Y. Wang, J. Zhu, D. Akinwande, N. Alem, J. A. Schuller, R. E. Schaak, M. Terrones, and J. A. Robinson, ACS Nano **9**, 11509 (2015).
[35]Z. Pang, J. Wan, A. Lu, J. Dai, L. Hu, and T. Li, Extrem. Mech. Lett. **35**, 100616 (2020).
[36]K. Wang, H. Li, and Y. Guo, Materials **14**, 4717 (2021).
[37]L. D. Williams, see https://williams.chemistry.gatech.edu/structure/molecular_interactions/mol_int.html for Molecular Interactions (aka Noncovalent Interactions, Intermolecular Forces) and the Behaviors of Biological Macromolecules (2021).
[38]S. Ramanayaka, M. Vithanage, A. Sarmah, T. An, K. H. Kim, and Y. S. Ok, RSC Adv. **9**, 34359 (2019).
[39]G. Deng, C. Tang, F. Li, H. Jiang, and Y. Chen, Macromolecules **43**, 1191 (2010).
[40]F. Lin, J. Yu, W. Tang, J. Zheng, A. Defante, K. Guo, C. Wesdemiotis, and M. L. Becker, Biomacromolecules **14**, 3749 (2013).
[41]J. Zhou, Z. Lin, H. Ren, X. Duan, I. Shakir, Y. Huang, and X. Duan, Adv. Mater. **33**, 2004557 (2021).
[42]L. Seidl, N. Bucher, E. Chu, S. Hartung, S. Martens, O. Schneider, and U. Stimming, Energy Environ. Sci. **10**, 1631 (2017).
[43]N. Feng, R. Meng, L. Zu, Y. Feng, C. Peng, J. Huang, G. Liu, B. Chen, and J. Yang, Nat. Commun. **10**, 1372 (2019).

[44]R. J. Moon, A. Martini, J. Nairn, and J. Youngblood, Chem. Soc. Rev. **40**, 3941 (2011).
[45]M. Henriksson, G. Henriksson, L. A. Berglund, and T. Lindström, Eur. Polym. J. **43**, 3434 (2007).
[46]H. Sehaqui, M. Allais, Q. Zhou, and L. A. Berglund, Compos. Sci. Technol. **71**, 382 (2011).
[47]M. Pääkko, M. Ankerfors, H. Kosonen, A. Nykänen, S. Ahola, M. Österberg, J. Ruokolainen, J. Laine, P. T. Larsson, O. Ikkala, and T. Lindström, Biomacromolecules **8**, 1934 (2007).
[48]T. Saito, S. Kimura, Y. Nishiyama, and A. Isogai, Biomacromolecules **8**, 2485 (2007).
[49]A. Isogai and Y. Zhou, Curr. Opin. Solid State Mater. Sci. **23**, 101 (2019).
[50]N. Sheng, S. Chen, M. Zhang, Z. Wu, Q. Liang, P. Ji, and H. Wang, ACS Appl. Mater. Interfaces **13**, 22416 (2021).
[51]J. Wei, B. Wang, Z. Li, Z. Wu, M. Zhang, N. Sheng, Q. Liang, H. Wang, and S. Chen, Carbohydr. Polym. **238**, 116207 (2020).
[52]C. Huang, H. Ji, Y. Yang, B. Guo, L. Luo, Z. Meng, L. Fan, and J. Xu, Carbohydr. Polym. **230**, 115570 (2020).
[53]R. T. Mackin, K. R. Fontenot, J. V. Edwards, N. T. Prevost, C. Grimm, B. D. Condon, F. Liebner, J. H. Jordan, M. W. Easson, and A. D. French, Cellulose **29**, 1293 (2022).
[54]N. Sheng, S. Chen, J. Yao, F. Guan, M. Zhang, B. Wang, Z. Wu, P. Ji, and H. Wang, Chem. Eng. J. **368**, 1022 (2019).
[55]Y. Wen, J. Liu, L. Jiang, Z. Zhu, S. He, S. He, and W. Shao, Food Packag. Shelf Life **29**, 100709 (2021).
[56]H. Shabbir, C. Dellago, and M. A. Hartmann, Biomimetics **4**, 12 (2019).
[57]C. H. Li and J. L. Zuo, Adv. Mater. **32**, 1903762 (2020).
[58]J. Cao, J. Li, Y. Chen, L. Zhang, and J. Zhou, Adv. Funct. Mater. **28**, 1800739 (2018).
[59]S. W. Wu, X. Liu, A. L. Miller, Y. S. Cheng, M. L. Yeh, and L. Lu, Carbohydr. Polym. **192**, 308 (2018).
[60]P. Song and H. Wang, Adv. Mater. **32**, 1901244 (2020).
[61]J. P. Gong, Y. Katsuyama, T. Kurokawa, and Y. Osada, Adv. Mater. **15**, 1155 (2003).
[62]L. Liu, Y. Liu, M. Tan, N. Che, and C. Li, Environ. Sci. Pollut. Res. **28**, 42637 (2021).
[63]Q. Zhang, M. Wu, X. Hu, W. Lu, M. Wang, T. Li, and Y. Zhao, Macromol. Chem. Phys. **221**, 1900320 (2020).
[64]H. Yuan, J. Xu, E. P. Van Dam, G. Giubertoni, Y. L. A. Rezus, R. Hammink, H. J. Bakker, Y. Zhan, A. E. Rowan, C. Xing, and P. H. J. Kouwer, Macromolecules **50**, 9058 (2017).
[65]R. Li, J. Lin, Y. Fang, C. Yu, J. Zhang, Y. Xue, Z. Liu, J. Zhang, C. Tang, and Y. Huang, Ceram. Int. **44**, 22439 (2018).
[66]L. Zhu, Y. Liu, Z. Jiang, E. Sakai, J. Qiu, and P. Zhu, Cellulose **26**, 5291 (2019).
[67]P. Song, B. Liu, C. Liang, K. Ruan, H. Qiu, Z. Ma, Y. Guo, and J. Gu, Nano-Micro Lett. **13**, 91 (2021).
[68]F. Jiang and Y. L. Hsieh, ACS Appl. Mater. Interfaces **9**, 2825 (2017).
[69]Z. Shang, D. Ding, X. Wang, B. Liu, Y. Chen, L. Gong, Z. Liu, and Q. Zhang, Polym. Adv. Technol. **32**, 4745 (2021).
[70]W. Zhang, H. Deng, L. Xia, L. Shen, C. Zhang, Q. Lu, and S. Sun, Carbohydr. Polym. **256**, 117507 (2021).
[71]Y. Shi, C. Liu, Z. Duan, B. Yu, M. Liu, and P. Song, Chem. Eng. J. **399**, 125829 (2020).
[72]Y. Li, H. Zhu, Y. Wang, U. Ray, S. Zhu, J. Dai, C. Chen, K. Fu, S.-H. Jang, D. Henderson, T. Li, and L. Hu, Small Methods **1**, 1700222 (2017).
[73]S. Keten, Z. Xu, B. Ihle, and M. J. Buehler, Nat. Mater. **9**, 359 (2010).
[74]Y. Dou, Z. P. Wang, W. He, T. Jia, Z. Liu, P. Sun, K. Wen, E. Gao, X. Zhou, X. Hu, J. Li, S. Fang, D. Qian, and Z. Liu, Nat. Commun. **10**, 5293 (2019).
[75]P. Song, Z. Xu, Y. Wu, Q. Cheng, Q. Guo, and H. Wang, Carbon **111**, 807 (2017).
[76]Y. Liu, B. Xie, Z. Zhang, Q. Zheng, and Z. Xu, J. Mech. Phys. Solids **60**, 591 (2012).
[77]A. S. Mahadevi and G. N. Sastry, Chem. Rev. **116**, 2775 (2016).
[78]J. Chen, Q. Peng, X. Peng, H. Zhang, and H. Zeng, Chem. Rev. **122**, 14594–14678 (2022).
[79]Z. Jia, Y. Yu, and L. Wang, Mater. Des. **168**, 107650 (2019).
[80]F. Barthelat, Z. Yin, and M. J. Buehler, Nat. Rev. Mater. **1**, 16007 (2016).
[81]S. M. Chen, H. L. Gao, X. H. Sun, Z. Y. Ma, T. Ma, J. Xia, Y. B. Zhu, R. Zhao, H. Bin Yao, H. A. Wu, and S. H. Yu, Matter **1**, 412 (2019).
[82]Z. B. Lai and C. Yan, J. Mech. Behav. Biomed. Mater. **65**, 236 (2017).
[83]T. V. Le, A. Ghazlan, T. Ngo, T. Nguyen, and A. Remennikov, Compos. Struct. **225**, 111172 (2019).
[84]X. Zeng, L. Ye, S. Yu, H. Li, R. Sun, J. Xu, and C. P. Wong, Nanoscale **7**, 6774 (2015).
[85]L. C. Zhou, Y. B. Zhu, Z. Z. He, X. Jin, and H. A. Wu, Compos. Struct. **259**, 113225 (2021).
[86]W. Fan, T. Du, A. Droce, L. R. Jensen, R. E. Youngman, X. Ren, L. Gurevich, M. Bauchy, P. Kristensen, B. Xing, D. Yu, and M. M. Smedskjaer, ACS Nano **16**, 9748 (2022).
[87]*Self-Healing and Self-Recovering Hydrogels*, edited by C. Creton and O. Okay (Springer), Vol. 285.
[88]A. GhavamiNejad, N. Ashammakhi, X. Y. Wu, and A. Khademhosseini, Small **16**, 2002931 (2020).
[89]Q. F. Guan, H. Bin Yang, Z. M. Han, Z. C. Ling, C. H. Yin, K. P. Yang, Y. X. Zhao, and S. H. Yu, ACS Nano **15**, 7889 (2021).
[90]J. P. Gong, T. Kurokawa, T. Narita, G. Kagata, Y. Osada, G. Nishimura, and M. Kinjo, J. Am. Chem. Soc. **123**, 5582 (2001).
[91]W. Zhang, X. Liu, J. Wang, J. Tang, J. Hu, T. Lu, and Z. Suo, Eng. Fract. Mech. **187**, 74 (2018).
[92]Q. Chen, X. Yan, L. Zhu, H. Chen, B. Jiang, D. Wei, L. Huang, J. Yang, B. Liu, and J. Zheng, Chem. Mater. **28**, 5710 (2016).
[93]T. Sedlačík, T. Nonoyama, H. Guo, R. Kiyama, T. Nakajima, Y. Takeda, T. Kurokawa, and J. P. Gong, Chem. Mater. **32**, 8576 (2020).
[94]X. Li, K. Cui, T. Kurokawa, Y. N. Ye, T. L. Sun, C. Yu, C. Creto, and J. P. Gong, Sci. Adv. **7**, eabe8210 (2021).
[95]X. Li, K. Cui, T. L. Sun, L. Meng, C. Yu, L. Li, C. Creton, T. Kurokawa, and J. P. Gong, Proc. Natl. Acad. Sci. U. S. A. **117**, 7606 (2020).
[96]D. D. McKinnon, D. W. Domaille, T. E. Brown, K. A. Kyburz, E. Kiyotake, J. N. Cha, and K. S. Anseth, Soft Matter **10**, 9230 (2014).
[97]R. Xiao, T. T. Mai, K. Urayama, J. P. Gong, and S. Qu, Int. J. Plast. **137**, 102901 (2021).
[98]J. Guo, M. Liu, A. T. Zehnder, J. Zhao, T. Narita, C. Creton, and C. Y. Hui, J. Mech. Phys. Solids **120**, 79 (2018).
[99]H. Wang, M. Cao, H. B. Zhao, J. X. Liu, C. Z. Geng, and Y. Z. Wang, Chem. Eng. J. **399**, 125698 (2020).
[100]G. Zu, T. Shimizu, K. Kanamori, Y. Zhu, A. Maeno, H. Kaji, J. Shen, and K. Nakanishi, ACS Nano **12**, 521 (2018).
[101]X. Zhang, W. Li, P. Song, B. You, and G. Sun, Chem. Eng. J. **381**, 122784 (2020).
[102]Y. Du, X. Zhang, J. Wang, Z. Liu, K. Zhang, X. Ji, Y. You, and X. Zhang, ACS Nano **14**, 11919 (2020).
[103]J. Zhu, J. Hu, C. Jiang, S. Liu, and Y. Li, Carbohydr. Polym. **207**, 246 (2019).
[104]J. Zhang, Y. Cheng, M. Tebyetekerwa, S. Meng, M. Zhu, and Y. Lu, Adv. Funct. Mater. **29**, 1806407 (2019).
[105]G. Zu, K. Kanamori, A. Maeno, H. Kaji, and K. Nakanishi, Angew. Chem. **130**, 9870 (2018).
[106]B. Wang, G. Li, L. Xu, J. Liao, and X. Zhang, ACS Nano **14**, 16590 (2020).
[107]Z. Liu, Y. Ran, J. Xi, and J. Wang, Soft Matter **16**, 9160 (2020).
[108]L. Wang, M. Zhang, B. Yang, J. Tan, and X. Ding, ACS Nano **14**, 10633 (2020).
[109]G. Zu, K. Kanamori, K. Nakanishi, and J. Huang, Chem. Mater. **31**, 6276 (2019).
[110]P. Hu, J. Lyu, C. Fu, W. Bin Gong, J. Liao, W. Lu, Y. Chen, and X. Zhang, ACS Nano **14**, 688 (2020).
[111]J. Zhu, S. Lv, T. Yang, T. Huang, H. Yu, Q. Zhang, and M. Zhu, Adv. Sustainable Syst. **4**, 1900141 (2020).

[112]H. J. Zhan, K. J. Wu, Y. L. Hu, J. W. Liu, H. Li, X. Guo, J. Xu, Y. Yang, Z. L. Yu, H. L. Gao, X. S. Luo, J. F. Chen, Y. Ni, and S. H. Yu, Chem **5**, 1871 (2019).
[113]W. Zhang, X. Xu, C. Zhang, Z. Yu, Y. Zhou, Y. Tang, P. Wu, and S. Guo, Small Methods **1**, 1700167 (2017).
[114]W. Dai, X. Niu, X. Wu, Y. Ren, Y. Zhang, G. Li, H. Su, Y. Lei, J. Xiao, J. Shi, B. Tong, Z. Cai, and Y. Dong, Angew. Chem. **134**, e202200236 (2022).
[115]X. Wang, J. Zhang, X. Mao, Y. Liu, R. Li, J. Bai, J. Zhang, C. Redshaw, X. Feng, and B. Z. Tang, J. Org. Chem. **87**, 8503 (2022).
[116]R. Liu and W. Li, ACS Omega **3**, 2609 (2018).
[117]X. Liao, M. Dulle, J. M. de Souza e Silva, R. B. Wehrspohn, S. Agarwal, S. Förster, H. Hou, P. Smith, and A. Greiner, Science **366**, 1376 (2019).
[118]Y. Wang, T. He, Z. Cheng, M. Liu, J. Ji, X. Chang, Q. Xu, Y. Liu, X. Liu, and J. Qin, Compos. Sci. Technol. **195**, 108204 (2020).
[119]X. Zhang, J. Chen, J. He, Y. Bai, and H. Zeng, J. Colloid Interface Sci. **585**, 420 (2021).
[120]S. Wu, M. Hua, Y. Alsaid, Y. Du, Y. Ma, Y. Zhao, C. Y. Lo, C. Wang, D. Wu, B. Yao, J. Strzalka, H. Zhou, X. Zhu, and X. He, Adv. Mater. **33**, 2007829 (2021).
[121]J. Suzuka, M. Tsuda, L. Wang, S. Kohsaka, K. Kishida, S. Semba, H. Sugino, S. Aburatani, M. Frauenlob, T. Kurokawa, J. Suzuka, M. Tsuda, L. Wang, S. Kohsaka, K. Kishida, S. Semba, H. Sugino, S. Aburatani, M. Frauenlob, T. Kurokawa, S. Kojima, T. Ueno, Y. Ohmiya, H. Mano, K. Yasuda, J. P. Gong, S. Tanaka, J. P. G, S. T. S. Kojima, T. Ueno, Y. Ohmiya, H. Mano, and K. Yasuda, Nat. Biomed. Eng. **5**, 914–925 (2021).
[122]C. Yang and Z. Suo, Nat. Rev. Mater. **3**, 125 (2018).
[123]D. Zhao, Y. Zhu, W. Cheng, G. Xu, Q. Wang, S. Liu, J. Li, C. Chen, H. Yu, and L. Hu, Matter **2**, 390 (2020).
[124]Z. Pang and T. Li, J. Mech. Phys. Solids **157**, 104626 (2021).
[125]M. G. Holland, Phys. Rev. **134**, A471 (1964).
[126]J. D. Chung, A. J. H. McGaughey, and M. Kaviany, J. Heat Transfer **126**, 376 (2004).
[127]L. Mu, J. He, Y. Li, T. Ji, N. Mehra, Y. Shi, and J. Zhu, J. Phys. Chem. C **121**, 14204 (2017).
[128]T. Zhou, C. Wu, Y. Wang, A. P. Tomsia, M. Li, E. Saiz, S. Fang, R. H. Baughman, L. Jiang, and Q. Cheng, Nat. Commun. **11**, 2077 (2020).
[129]Y. Zhang and X. Li, Nano Lett. **17**, 6907 (2017).
[130]L. Wang and T. Chen, Compos. Part A **161**, 107097 (2022).
[131]D. Yuan, X. Yang, S. Wu, S. Lü, and K. Hu, J. Mater. Process. Technol. **269**, 1 (2019).
[132]R. Ma, W. Li, M. Huang, M. Feng, and X. Liu, Compos. Sci. Technol. **170**, 128 (2019).
[133]Y. Lu, S. Su, S. Zhang, Y. Huang, Z. Qin, X. Lu, and W. Chen, Acta Mater. **206**, 116632 (2021).
[134]W. Xie and Y. Wei, Nano Lett. **21**, 4823 (2021).
[135]Y. Hou, Q. Guan, J. Xia, Z. Ling, Z. He, Z. Han, H. Yang, P. Gu, Y. Zhu, S. Yu, and H. Wu, ACS Nano **15**, 1310-1320 (2020).
[136]R. Wang, C. Chen, Z. Pang, X. Wang, Y. Zhou, Q. Dong, M. Guo, J. Gao, U. Ray, Q. Xia, Z. Lin, S. He, B. Foster, T. Li, and L. Hu, Nano Lett. **22**, 3931 (2022).
[137]N. C. Sekhar and L. A. Varghese, Polym. Test. **79**, 106010 (2019).
[138]T. Cai, Y. Z. Yan, Y. Park, T. Lee, D. Peng, Y. Liu, C. S. Ha, and K. C. Kim, ACS Appl. Polym. Mater. **3**, 2461 (2021).
[139]J. Wang, J. He, L. Ma, Y. Zhang, L. Shen, S. Xiong, K. Li, and M. Qu, Chem. Eng. J. **390**, 124508 (2020).
[140]K. Yang, J. He, Q. Zhou, X. Hao, H. Yang, and Y. You, Polymer **214**, 123354 (2021).
[141]Y. Zhu, Z. Yu, J. Zhu, Y. Zhang, X. Ren, and F. Jiang, Chem. Eng. J. **445**, 136748 (2022).
[142]T. Saito, R. Kuramae, J. Wohlert, L. A. Berglund, and A. Isogai, Biomacromolecules **14**, 248 (2013).
[143]R. M. A. Domingues, M. E. Gomes, and R. L. Reis, Biomacromolecules **15**, 2327 (2014).
[144]S. Iwamoto, W. Kai, A. Isogai, and T. Iwata, Biomacromolecules **10**, 2571 (2009).
[145]A. Šturcová, G. R. Davies, and S. J. Eichhorn, Biomacromolecules **6**, 1055 (2005).
[146]R. T. Olsson, M. A. S. Azizi Samir, G. Salazar-Alvarez, L. Belova, V. Ström, L. A. Berglund, O. Ikkala, J. Nogués, and U. W. Gedde, Nat. Nanotechnol. **5**, 584 (2010).
[147]J. Song, C. Chen, S. Zhu, M. Zhu, J. Dai, U. Ray, Y. Li, Y. Kuang, Y. Li, N. Quispe, Y. Yao, A. Gong, U. H. Leiste, H. A. Bruck, J. Y. Zhu, A. Vellore, H. Li, M. L. Minus, Z. Jia, A. Martini, T. Li, and L. Hu, Nature **554**, 224 (2018).
[148]J. Chung, A. M. Kushner, A. C. Weisman, and Z. Guan, Nat. Mater. **13**, 1055 (2014).
[149]H. Xing, Z. Li, W. Wang, P. Liu, J. Liu, Y. Song, Z. L. Wu, W. Zhang, and F. Huang, CCS Chem. **2**, 513 (2020).
[150]J. Fish, G. J. Wagner, and S. Keten, Nat. Mater. **20**, 774 (2021).
[151]C. P. Gomes, D. Fink, R. B. van Dover, and J. M. Gregoire, Nat. Rev. Mater. **6**, 645 (2021).
[152]S. Zhou, K. Jin, and M. J. Buehler, Adv. Mater. **33**, 2003206 (2021).
[153]M. Wang, T. Wang, P. Cai, and X. Chen, Small Methods **3**, 1900025 (2019).
[154]D. C. Elton, Z. Boukouvalas, M. S. Butrico, M. D. Fuge, and P. W. Chung, Sci. Rep. **8**, 9059 (2018).
[155]D. P. Metcalf, A. Koutsoukas, S. A. Spronk, B. L. Claus, D. A. Loughney, S. R. Johnson, D. L. Cheney, and C. D. Sherrill, J. Chem. Phys. **152**, 074103 (2020).
[156]Z. Yang, C. H. Yu, K. Guo, and M. J. Buehler, J. Mech. Phys. Solids **154**, 104506 (2021).
[157]K. T. Schütt, M. Gastegger, A. Tkatchenko, K. R. Müller, and R. J. Maurer, Nat. Commun. **10**, 5024 (2019).
[158]D. J. Cole, L. Mones, and G. Csányi, Faraday Discuss. **224**, 247 (2020).
[159]P. Gasparotto and M. Ceriotti, J. Chem. Phys. **141**, 174110 (2014).
[160]K. Hansen, F. Biegler, R. Ramakrishnan, W. Pronobis, O. A. Von Lilienfeld, K. R. Müller, and A. Tkatchenko, J. Phys. Chem. Lett. **6**, 2326 (2015).
[161]C. A. Bauer, G. Schneider, and A. H. Göller, J. Cheminform. **11**, 59 (2019).
[162]S. Wang, H. S. Pillai, and H. Xin, Nat. Commun. **11**, 6132 (2020).